Steady State and Transient Response Characteristics of Commercial Carbon Monoxide Sensors

by

Amy Leigh Buck

A thesis submitted to the Graduate Faculty of
Auburn University
in partial fulfillment of the
requirements for the Degree of
Master of Science

Auburn, Alabama
May 4, 2014

Keywords: Airline Cabin Environment Research (ACER), Carbon Monoxide, Electrochemical Sensor

Approved by

Ruel A. Overfelt, Chair, Professor of Mechanical Engineering
Bart Prorok, Professor of Mechanical Engineering
Jeffrey Fergus, Professor of Mechanical Engineering

Abstract

Suggestions have been made to include sensor platforms that are capable of detecting potential bleed air contamination events on commercial airliners to protect the health and safety of aircraft passengers and crew. Detecting high levels of carbon monoxide in the bleed air system of an aircraft may indicate a contamination event since many of the suspected bleed air contaminants evolve carbon monoxide at the elevated temperatures seen in the compressor stages of the engine. Because the levels of carbon monoxide are not expected to reach a steady-state during a transitory contamination event, it is important to understand the transient response characteristics of carbon monoxide sensors. Several electrochemical carbon monoxide sensors were tested in a chamber designed to provide an almost instantaneous gas concentration change. The sensors were evaluated for their response time and accuracy. The sensors' initial response rates were found to be linear with respect to the imposed concentrations and this characteristic may enable estimates of the levels of contamination events due to brief indications of high levels of carbon monoxide.

Acknowledgements

I would like to convey my sincere appreciation to Dr. Overfelt for all of his assistance and guidance on this project and my graduate education as a whole. I would also like to thank Dr. Prorok and Dr. Fergus for serving on my committee and their guidance through this project. I would like to thank Dr. Duke for his guidance.

I also want to thank all of my colleagues for all of their assistance on this project. I would like to thank Matthew Roberts and Bethany Brooks who were always willing to help in any way possible. I also want to thank Naved Siddiqui for his assistance. I would like to say thank you to John Andress who was invaluable in helping me get started at the beginning of this project. I would also like to express gratitude to Vignesh Venkatasubramanian and Hassan Sk for all of their assistance as well. Finally I would like to say thank you to Mike Crumpler for all of his technical expertise, patience and support on this project.

Most of all, I want to thank my husband, MacGyver, for all of his patience and support through this time.

This project was partially funded by the U.S. Federal Aviation Administration (FAA) Office of Aerospace Medicine through the National Air Transportation Center of Excellence for Research in the Intermodal Transport Environment (RITE), Cooperative Agreement 10-C-RITE-AU. Although the FAA has sponsored this project, it neither endorses nor rejects the findings of this research.

Table of Contents

List of Tables

List of Figures

Nomenclature

ACGIH	American Conference of Governmental Industrial Hygienists
CO	Carbon Monoxide
CO_2	Carbon Dioxide
$\mathcal{E}$	Volts
FAA	Federal Aviation Administration
GDE	Gas Diffusion Electrode
HEPA	High Efficiency Particulate Air
N_2	Nitrogen gas
NIOSH	National Institute for Occupational Safety and Health
O_2	Oxygen gas
OSHA	Occupational Safety and Health Administration
ppb	parts per billion
ppm	parts per million
PTFE	Polytetrafluoroethylene
RMS	Root Mean Square
SPE	Solid Polymer-electrolyte Electrode
VOC	Volatile Organic Compound

1. Introduction

Gas detection is a vital safety precaution in many industries. The ability to quickly and reliably detect potentially toxic gases is critical to keep people safe. Environments where occupants are in enclosed spaces are particularly dangerous if toxic gases are present. Buildings, automobiles, submarines, mines, and aircraft cabins are some of the potentially dangerous enclosed spaces.

The enclosed environment of an airliner cabin is the focus in this study and air quality is vital to crew and passenger safety and comfort. For most airliners the cabin air is provided through the bleed air system of the aircraft. The bleed air system pulls compressed air from the compressor stage of one or more of the turbine engines used for propulsion and power on the aircraft. The air from the turbine compressor passes through heat exchangers and an air conditioning pack. The cooled bleed air from outside the plane then enters a mixing unit where it is mixed with recirculated internal cabin air. The mixed air then passes through a HEPA filter and enters the cabin. This process is shown in Figure 1 [1]. The bleed air system is vital to providing fresh air and keeping the cabin pressurized at a survivable pressure during flight which keeps passengers comfortable and safe [2].

While the bleed air system is critical to keeping people in a safe environment at cruise altitude, there is a potential for degraded air quality. After complaints from passengers and crew, the National Research Council twice opened investigations into the

air quality in airline cabins. In order to improve air quality, the first investigation in 1986 led to a ban on smoking on short domestic flights. The FAA also reduced the acceptable level of CO_2 from 30,000 ppm to 5000 ppm. Continued pressure from labor unions has kept open the issue of air quality in commercial airliners [2].

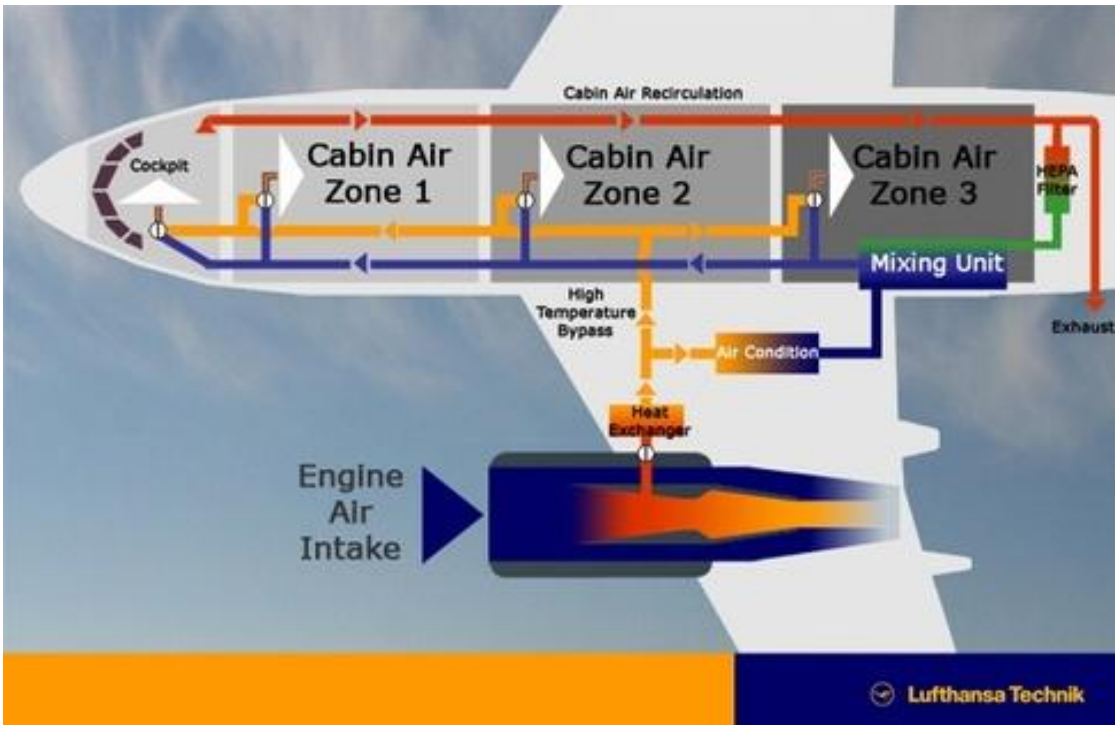

Figure 1: Airliner bleed air system schematic [1]

Although bleed air contamination events appear to be rare, there are documented cases where contamination of the airline cabin air has occurred. A British government study showed that crew reported air contamination events in up to 1% of flights. However maintenance records showed a much lower occurrence on only 0.05% of flights. With nearly 28,000 flights in the US every day, such rates would amount to several flights each day with potential bleed air contamination events. According to the

FAA over 900 bleed air fume events were recorded between 1999 and 2008 [3]. These events are also believed to have caused crew members to lose flight clearances [4].

The sources of contaminants in bleed air events are thought to be from engine fluids, such as hydraulic fluid or engine oil, deicing fluid or exhaust from ground vehicles and other aircraft [5]. Engine oils have been shown to thermally degrade into CO, CO_2, and VOC's depending upon the specific exposure temperature and time [6]. CO has been identified as the primary contaminant of interest in this study.

CO sensors are common and available from many manufacturers. Commercially available CO sensors usually rely on electrochemical or metal oxide semiconductor technology. Electrochemical sensors were chosen due to their long term stability and linearity in response to CO concentrations. Three electrochemical sensors were chosen and the steady state performances as well as the transient response characteristics were determined. Several different CO concentrations were applied to the sensors to test the response over a range of concentrations. A test chamber and associated experimental procedures were developed to enable characterization of the transient response of the sensor due to suddenly changed environmental conditions.

2. Literature Review

2.1 Aircraft Cabin Environment

The outside environment at typical cruise altitudes cannot support human life. At a typical cruise altitude of 41,000 ft the outside pressure is 3.65 lb/ft^2 and the temperature is less than -70° F [7]. The environmental control system (ECS) of an aircraft enables the survival of passengers and crew in these harsh conditions. In order to pressurize the cabin to a comfortable pressure, pressurized air is "bled off" the turbine compressor of the jet engines. The FAA requires that the cabin be kept at a pressure that is equal to or higher than the pressure at 8000 ft (i.e., 75 kPa or 10.9 psi). The percentage of oxygen in the air remains the same in the airline cabin as on the ground – around 21 percent. The problem that occurs is that the partial pressure of oxygen drops with the decreased overall pressure and it is the oxygen partial pressure that controls the level of blood oxygen saturation. So although the relative amount of oxygen remains the same, the absolute amount of oxygen available decreases [5].

The bleed air system of an aircraft is a complex system that is vital to the survivability of the aircraft environment. See Figure 2. On most commercial jet engines there are two bleed ports: a low pressure port and a high pressure port. The low pressure port is used for to extract bleed air when the engine power settings are at high levels while the high pressure port is used for low engine power settings. This ensures the pressure supplied to the bleed air system stays within easily controllable values. Due to

ozone that exists in the upper atmosphere the air coming through the bleed air system first passes through ozone converters to eliminate this harmful gas. The bleed air then enters air conditioning packs where the air is dried and sterilized. The air conditioning packs then supply air at the correct temperature and pressure for the cabin. This conditioned air is then mixed with recirculated air from the cabin. On some aircraft, the air also can be passed through HEPA filters to remove particulates and microorganisms before reentering the cabin [8], [9], [5].

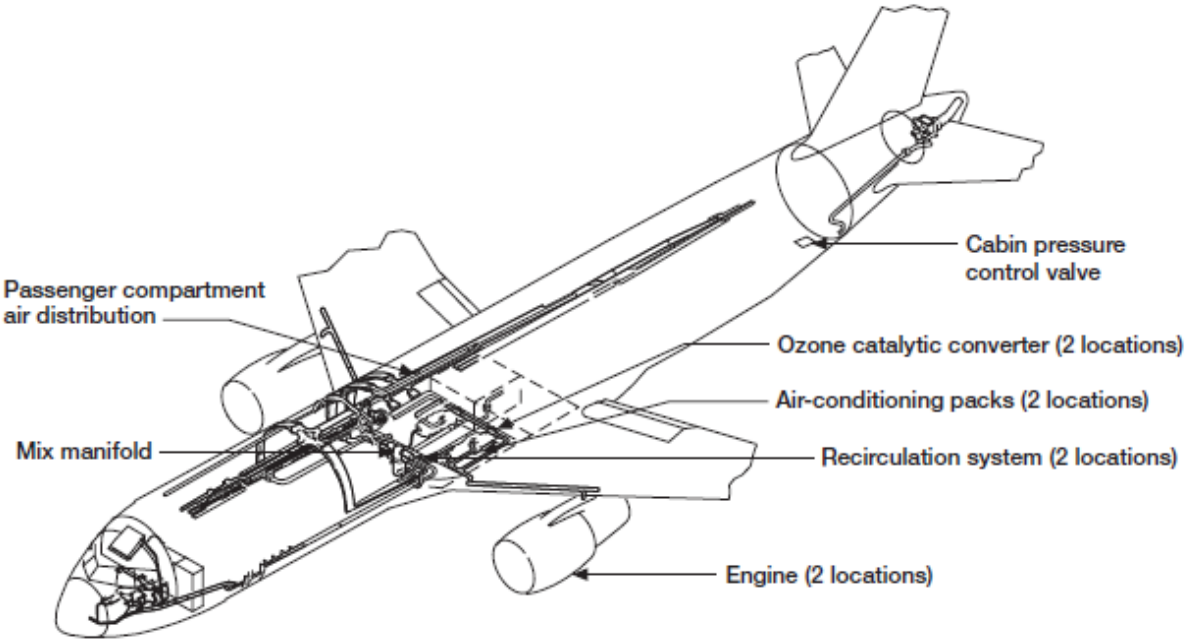

Figure 2: The aircraft bleed air system [8]

2.2 Possible Bleed Air Contaminants

The design of the bleed air system allows the potential for contamination of the air inside the cabin. Oil leaking from jet engine bearing seals, hydraulic fluid leaking

from seals, and environmental contaminants from the exhaust of ground support vehicles or other aircraft can enter the bleed air supply [5], [9]. Once engine oil or hydraulic fluid enters the bleed air system the elevated temperatures can cause them to degrade. These fluids have the potential to release CO, CO_2 and VOCs into the air stream as they decompose [6],[9]. These potentially dangerous gases are not filtered by HEPA filters and would enter the cabin if allowed into the bleed air supply.

2.3 Carbon Monoxide Hazards

Research has shown that the decomposition of engine oils can release a significant amount of CO [6], [10]. CO is especially dangerous at high altitudes. The effects of CO are intensified by the reduced oxygen environment of the aircraft cabin.

Carbon monoxide is a colorless, odorless gas that can lead to illness or even death. CO poisoning leads to 4,000 hospitalizations each year and results in 400 deaths. The CO molecules bind to the red blood cells and block the oxygen from binding as shown in Figure 3. This lack of oxygen causes tissue damage and death [11]. Symptoms of CO poisoning vary by person and by exposure level. Moderate CO exposure can lead to headache, fatigue, shortness of breath, nausea and dizziness. High CO exposure can lead to mental confusion, vomiting, loss of muscular coordination, loss of consciousness, and death [12]. These symptoms can become more severe with the low oxygen content of the aircraft cabin.

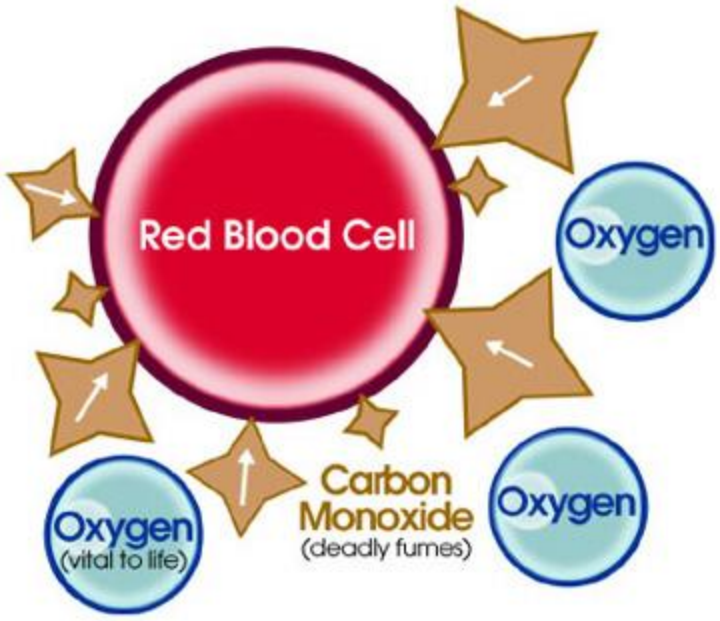

Figure 3: CO binds to red blood cells preventing oxygen from binding [11]

Regulations exist to control the amount of CO to which people can be exposed on aircraft. FAA regulations state that "crew and passenger compartment air must be kept free from harmful or hazardous concentrations of gases or vapors" [13]. The specific carbon monoxide concentration is not to exceed 1 part in 20,000 or 50 ppm [13]. The FAA does not control either (i) how the industry meets the limitation or (ii) whether the industry even monitors the level of CO in aircraft. Other workplace CO regulations are shown in Table 1. The exposure regulations for OSHA, NIOSH, and ACGIH are more specific than the FAA regulation.

Table 1: Federal CO concentration regulations [14]–[16]

Regulation	*8 Hour TWA (ppm)*	*Ceiling (ppm)*
FAA	NA	50
OSHA PEL	50	NA
NIOSH	35	200
ACGIH	25	NA

2.4 Electrochemical Detection of Carbon Monoxide

Electrochemical detection is the most common type of carbon monoxide detection. The basic process steps for electrochemical detection are shown in Figure 4. The gaseous analyte must first diffuse to the electrode where it adsorbs and undergoes an electrochemical reaction generating a measurable electrical signal. After the electrochemical reaction, the products diffuse away [17].

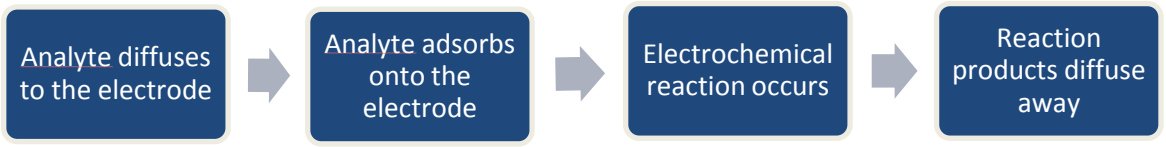

Figure 4: Basic process steps of electrochemical detection (adapted from [17])

Figure 5 shows two types of electrochemical cells that can be used for detection of gaseous species. Gas diffusion electrodes (GDE) are based on PTFE-bonded metal and solid polymer-electrolyte electrodes (SPE) use a porous metal layer boded to an ion conducting membrane [17].

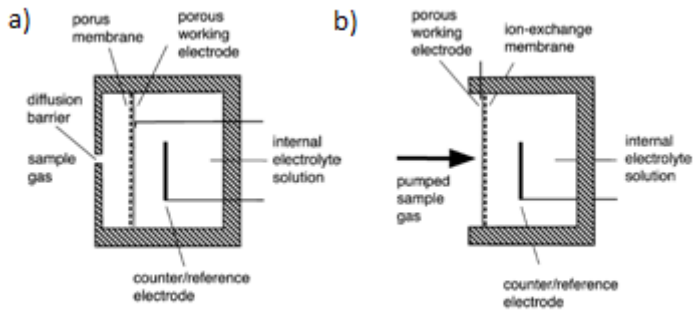

Figure 5: Types of electrochemical cells a. gas diffusion electrode (GDE) b. solid polymer-electrolyte electrode (SPE) [17]

. The GDE is a common amperometric gas sensor design. Because the electrolyte is in direct contact with the electrodes, mass transfer occurs quickly resulting in short sensor response times. This sensor design is a mature technology that has been incorporated in many devices. The SPE is a newer sensor design developed in the 1980s. One of the major differences between the SPE and GDE is the way the analyte gas is introduced. The GDE relies upon gas diffusion while the SPE design actively pumps the gas.

Commercially available electrochemical CO sensors are mostly the GDE type. These sensors work by producing a current that is proportional to the amount of analyte. A typical sensor is shown in Figure 6. There are three electrodes in a typical amperometric CO sensor. The working electrode is where the electrochemical oxidation reaction of the CO gas occurs. The working electrode facilitates the gas contacting the electrocatalyst and the electrolyte simultaneously. The electrolyte is generally sulfuric acid and allows the ions to flow between the working and counter electrodes. The counter electrode serves to balance the reaction that occurs at the working electrode. For CO, the reactions at each electrode are shown in Equations (1)-(3). Equation (1) illustrates the

reaction at the working electrode, Equation (2) describes the reaction at the counter electrode, and Equation (3) is the overall reaction [18].

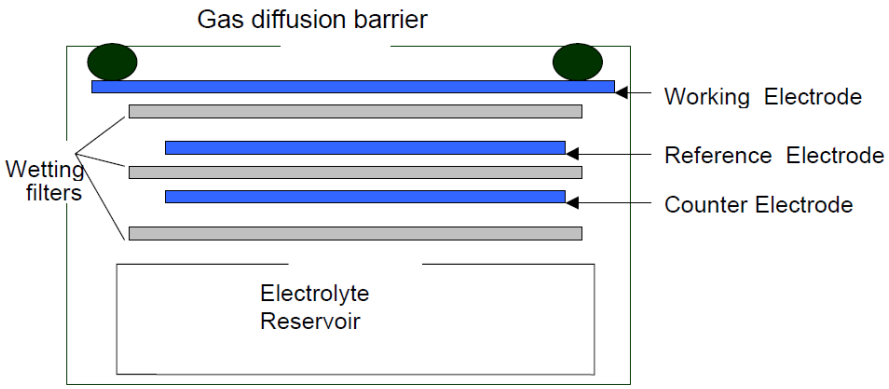

Figure 6: Schematic of a typical 3 electrode electrochemical sensor [18]

$$CO + H_2O \rightarrow CO_2 + 2H^+ + 2e^- \quad (1)$$

$$½\ O_2 + 2H_2 + 2e^- \rightarrow H_2O \quad (2)$$

$$CO + ½\ O_2 \rightarrow CO_2 \quad (3)$$

Most electrochemical sensors also include a third electrode, as a reference electrode. The reference electrode holds the working electrode potential constant so that the working electrode stays in the plateau region of the current-voltage curve shown in Figure 7 [18]. This plateau is where the electrochemical reaction is diffusion limited and maintaining the working electrode in this region keeps the sensor response linearly dependent on concentration. If the working electrode leaves this plateau the reaction kinetics become important and begin influencing reaction timing and the sensor response

becomes non-linear with concentration. The sensor also becomes more prone to aging effects [18],[17].

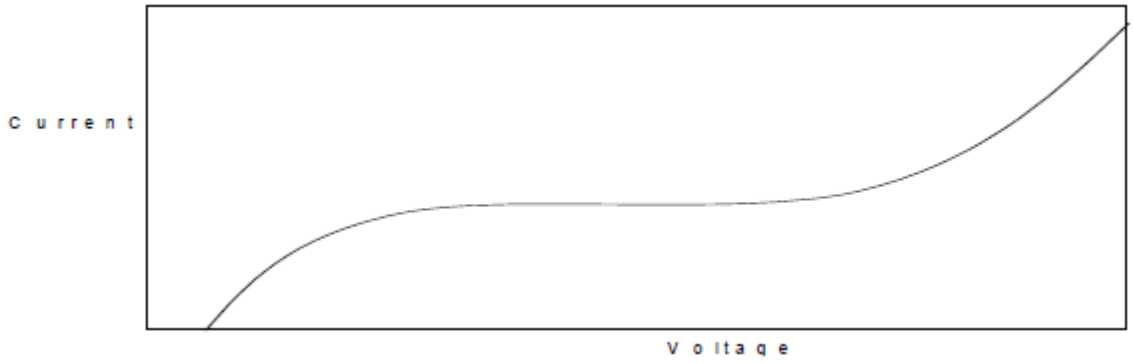

Figure 7: Schematic Electrochemical sensor current-voltage curve [17]

2.5 Measurement Uncertainties with Electrochemical Sensors

Uncertainty estimates for chemical measurements using electrochemical methods are often complex. There are several sources of uncertainty that must be accounted for to get an accurate measurement from an electrochemical gas sensor [19].

Temperature compensation is the first source of uncertainty. The rates of diffusion and the electrochemical reaction itself are both affected by temperature. Temperature poses two problems for uncertainty measurement. The first is the measurement of the temperature brings about uncertainty in both the calibration and the measurement stages. The second is the temperature compensation built into the commercial sensor. The factors used to compensate for temperature differences can themselves bring about uncertainty [19].

Sensor drift can also be a large source of uncertainty. The sensor response can change over time due to changes in the sensor. For example, sensor response can drift due to unstable electrode potential or consumption of the electrolyte or electrodes. Poisoning can also affect the drift of the sensor if the sensor is exposed to high concentrations or other gases that interfere with components.

Flow rate can also influence the results of the sensor. The flow rate can alter the boundary layer between the gas and the membrane. This boundary layer change alters the analyte the sensor 'sees' because the sensor is only reading the stagnant boundary layer. A change in thickness of this boundary layer will alter the amount of gas the sensor reads [19].

The response time can affect the uncertainty if the sensor is not allowed to reach steady state before a measurement is taken. Response times are commonly specified as the time it takes for a sensor to reach 90% of the steady state value. Gas diffusion is the limiting step in the reaction process making it the limiting step for the sensor response time. This uncertainty source is easily eliminated during calibration tests by ensuring the sensor can reach steady state [19]. However, measurements of dynamic processes like bleed air contamination events in real aircraft never reach steady state and require careful measurement procedures and interpretation of results.

The linearity of the sensor can also be a source of uncertainty. A non-linear sensor is very hard to calibrate and the uncertainty between calibration and measurement increases as the nonlinearity increases [19]. The nonlinearity can be controlled by ensuring diffusion is the rate limiting step in most electrochemical sensors [17].

The analyte concentration during calibration can be another major source of uncertainty. If the concentration of the analyte during calibration is uncertain the measurements later will only be as good as the precision of the calibration. It is important to use a high precision analyte concentration during calibration [19].

Interference is the last major source of uncertainty. Most electrochemical sensors are at least partially sensitive to compounds other than the desired analyte. Since calibration is generally done with pure gas mixtures with no interfering gases, any time the sensor is used in the presence of an interfering gas, the sensor reading will contain some uncertainty. This uncertainty can sometimes be compensated by removing the interfering gas or measuring the interfering gas alone with no analyte and then adjusting the zero current to account for the interference [19].

3. Experimental Procedures

3.1 Commercial Electrochemical Sensors

Several companies manufacture sensors to detect carbon monoxide. Many of these sensors are designed for home or industrial safety or for monitoring manufacturing processes. The sensors designed to monitor manufacturing processes generally detect much higher levels of carbon monoxide than would be present in a home, building, or aircraft cabin.

Three sensors were chosen for evaluation in this work: (i) the CO-B4 sensor manufactured by Alphasense, (ii) the TGS5042 device manufactured by Figaro Inc. and (iii) the EC4-500-CO sensor manufactured by e2v Technologies (now SGX Sensortech). All three sensors and evaluation boards are relatively small as shown in Figure 8. The important specifications for these devices were compiled from their manufacturers and are shown in Table 2. The "full scale ppm" data shown in Table 2 represents the maximum CO concentration that each sensor can display.

Alphasense notes that the CO-B4 technology is a reliable sensor for use where ppb detection levels are required. With a lower detection limit of less than 20 ppb, this sensor is reported by the manufacturer as ideal for use in applications where very small concentrations of CO need to be detected. This sensor incorporates technology to maximize the signal-to-noise ratio and low zero currents to reach such low readings [20].

Figaro's TGS5042 device was chosen because of its use in many commercial CO detectors for residential and commercial buildings. Figaro states that the TGS5042 is ideal for these applications because of it has (i) low power requirements,(ii) good repeatability, (iii) high selectivity, and (iv) a life of up to 7 years under normal residential conditions [21].

The EC4-500-CO sensor from e2v Technologies was chosen for its similarity with Figaro's TGS5042 and its wide spread use in industrial CO detectors. The EC4-500-CO was the only sensor tested with industry standard connections for use in gas monitors. This sensor also has low power consumption and a fast response [22].

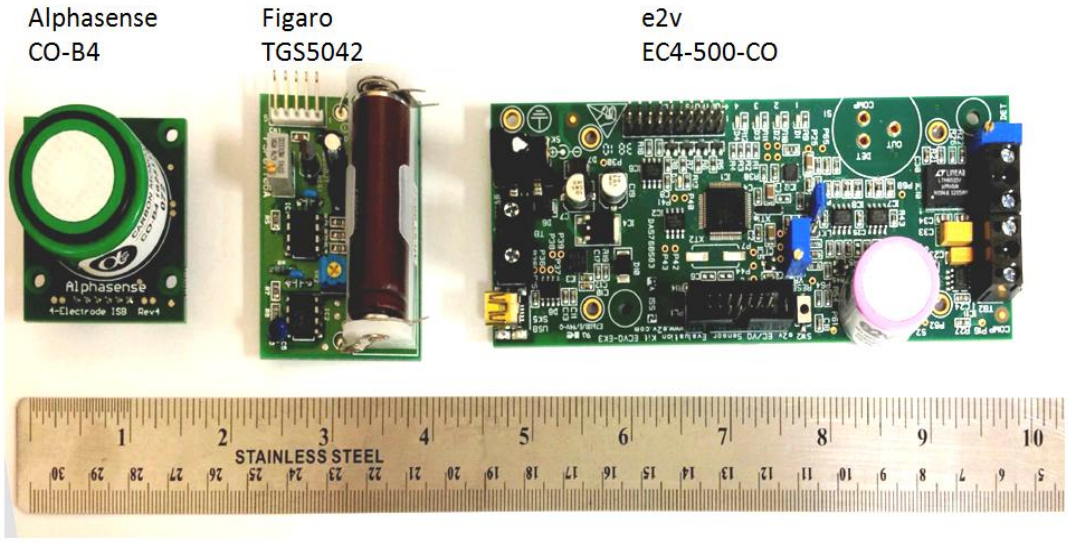

Figure 8: Sensors and evaluation boards investigated in this work: Alphasense CO-B4, Figaro TGS5042 and e2v EC4-500-CO

Table 2: Sensor Manufacturer specifications [20], [21], [23]

Manufacturer	*Sensor Name*	*Evaluation Board*	*Full Scale CO ppm*	*Sensitivity (nA/ppm CO)*	*Manufacturer Response Time*	*CO Resolution*
Alphasense	CO-B4	4 Electrode ISB	13	300-500	t_{90} < 25 s	< 5 ppb
Figaro	TGS 5042	COM5042	10,000	1.2-2.4	t_{90} < 60 s	NA
e2v	EC4-500-CO	ECVQ-EK3	500	55-85	t_{90} < 30 s	1 ppm

3.2 Test Gas Compositions

Calibration gas mixtures of CO were supplied from premixed tanks of various CO concentrations and a balance of nitrogen from AirGas Inc, Opelika, AL. Certificates of the gas compositions are shown in Appendix A. CO Concentrations were 18, 50, 70, 100, and 250 ppm. The concentrations in ppm were converted to mg/m^3 in this study for more precise comparisons with measurements in an aircraft where decreased pressures are likely. Thus the concentrations of the premixed calibration gases used here (at standard temperature and pressure) are 21, 58, 82, 116, and 291 mg/m^3.

3.3 Test Apparatus

Two test chambers were designed and fabricated to enable testing of each sensor individually as well as all three sensors simultaneously.

3.3.1 Small Test Chamber

A small 4 inch diameter acrylic chamber with a volume of 2.5 L was developed for steady state measurements of gas sensor response (as well as used for preliminary trials of transient testing, see below). Test plugs were used to seal both ends of an acrylic

tubular chamber as shown in Figure 9. A small fan was mounted to one of the test plugs to provide mixing of the test gases. The small test chamber enabled precision measurements of each sensor steady state response to the certified test gas compositions while minimizing the amount of certified gas required. For calibration of the Figaro TGS5042 and e2v EC4-500-CO, the calibration gas flowed directly from the premixed tanks through the small test chamber and to the building exhaust.

Figure 9: Small test chamber

3.3.1 Large Test Chamber

The steady state and transient response of each sensor to an "instantaneous" change in CO concentration was evaluated using a larger test chamber with a total volume of 16.7 L. The experimental procedures discussed below allowed the temporal response of each sensor to be evaluated without complicating issues involving a sensor "chasing" a time varying gas concentration. The desired "instantaneous" step function concentration change and the expected sensor response are shown schematically in Figure 10.

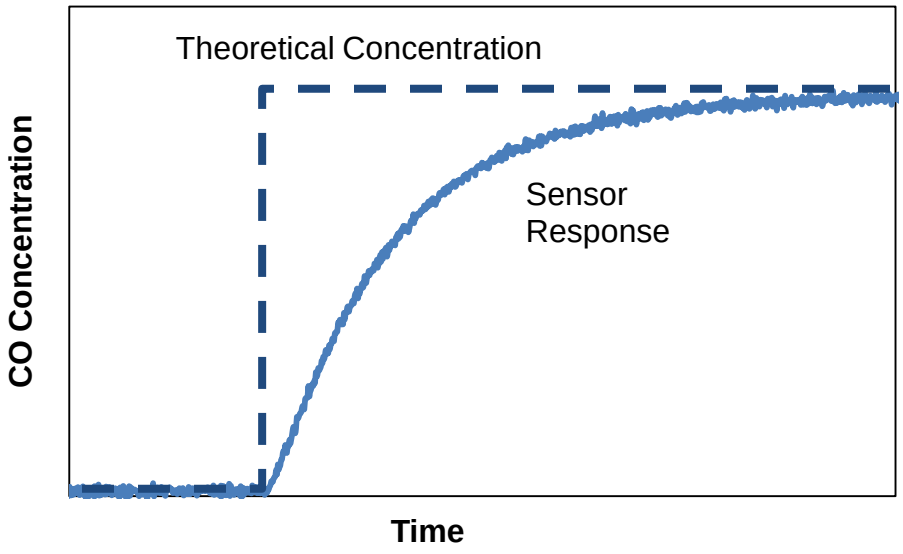

Figure 10: A schematic of the desired instantaneous gas concentration profile (dashed line) compared with an expected sensor response (solid line)

A schematic of the transient response test apparatus is shown in Figure 11. As noted above, the test gas was supplied from pre-mixed tanks of specified concentrations of CO with a balance of nitrogen. The gas was then passed through a flow meter to control and measure the flow from the gas cylinders. A pressure transducer was used to

monitor the gas pressure inside the inflatable bladder. The thin membrane bladder was used to contain the gas until it was mechanically burst and the test gas released into the test chamber. A sharp tool, inserted through the opening shown in Figure 11, was used to burst the bladder. A rubber stopper was then quickly placed into the opening to seal the chamber. This sealed the chamber for the duration of the test. Ball valves were used to isolate the chamber during testing and, once a test was completed, clean laboratory air was used to purge the chamber into the building exhaust system.

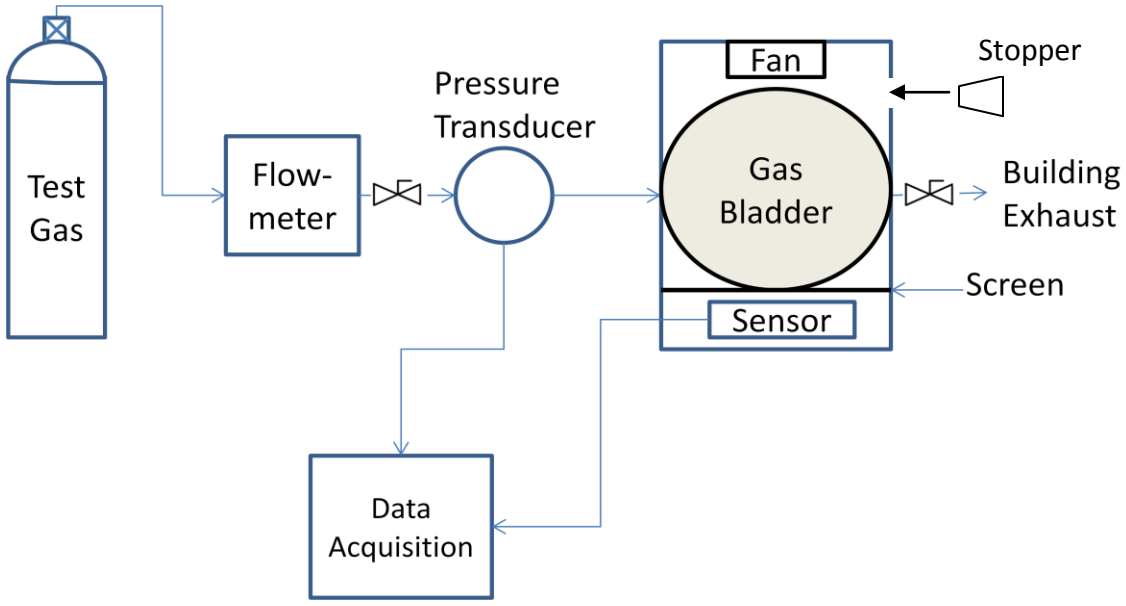

Figure 11: Test arrangement schematic. The test gas flows from a premixed pressurized tank through a flow meter and pressure transducer to a gas bladder inside the test chamber.

The transient response test chamber consisted of a 10 inch diameter acrylic tube with a plate bonded to one end and a removable test plug to seal the other end. Fans were mounted to the test plug to provide circulation to aid in the mixing of the gas with the residual air in the test chamber. A metal screen was mounted at the bottom of the

chamber between the inflatable bladder and the sensors to prevent the bursting of the bladder from damaging any of the sensors.

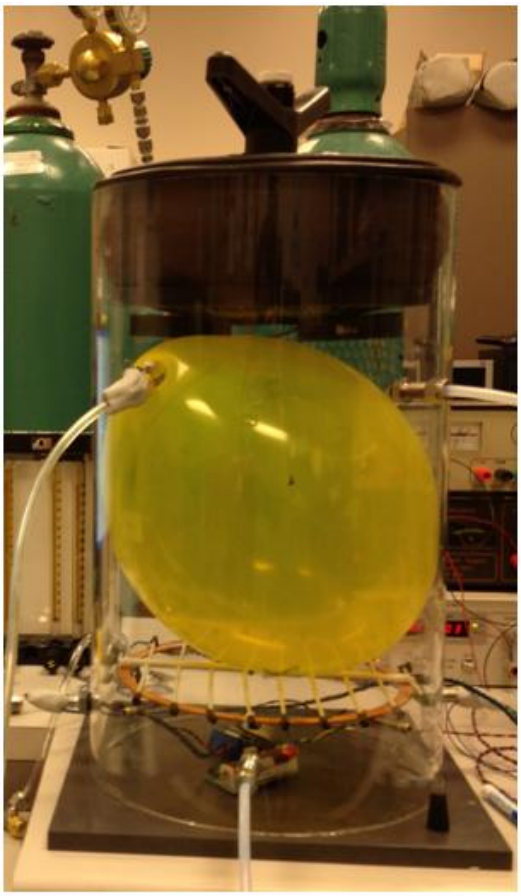

Figure 12: Transient response test chamber

The test chamber was leak tested to ensure the concentration of the gas in the chamber remained constant. The chamber was filled with gas and sealed and then the concentration was monitored for 12 minutes. Experiments typically were run for either 5 or 10 minutes so 12 minutes was longer than the expected duration of any test. Typical

results of both a leaking chamber and a well-sealed chamber are shown in Figure 13. Leaking chambers were easily identified and corrected prior to all sensor tests.

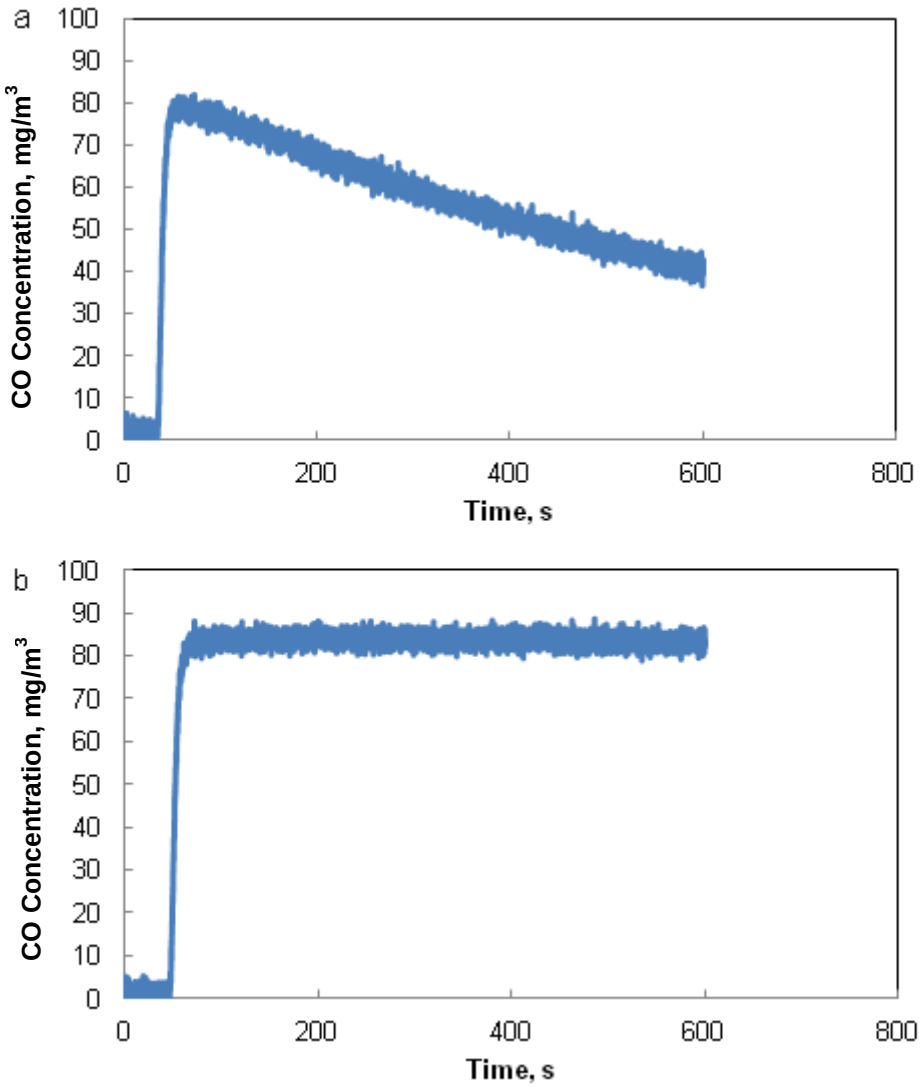

Figure 13: Comparison between: a) typical leaking and b) sealed chamber. Tests were completed at 80 mg/m^3 CO.

The adequacy of gas mixing after bladder bursting was investigated using a Motion Scope M2 by Redlake, Cheshire, CT. Figure 14 shows high speed video footage

taken of a bladder filled with test gas and also containing a large number of reflective particles to enable visualization of the gas mixing effects immediately after bladder rupture. The video was filmed at 250 fps and the 12 frames shown in the image were taken over 0.048 seconds total. The first two frames are before the bladder was burst and frame 3 is just when the bladder bursts and the particles are released. The reflective particles appear to fill the chamber quickly after bladder bursting.

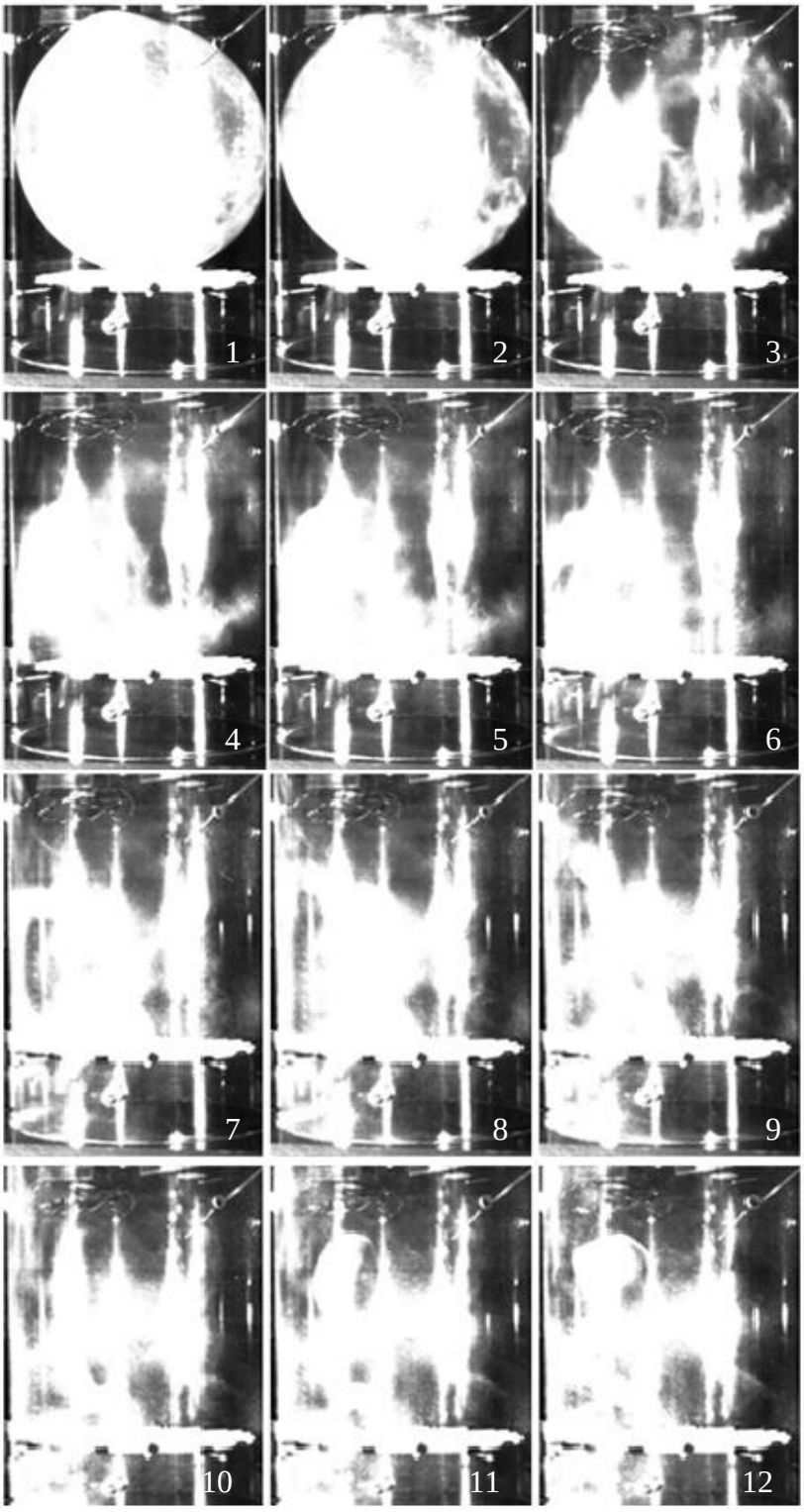

Figure 14: High speed image capture of reflective particles released from a burst bladder. Images were taken at 250 fps. Note bladder bursting in image 3.

Response times for the TGS5042 sensor instantaneously exposed to various levels of CO gas concentration are shown in Table 3. The scatter and large standard deviations in these data indicated that mixing of the test gas with the residual air might not be repeatable from experiment to experiment. A small fan was added to the test chamber and a series of experiments were conducted to vary the fan speed to enhance mixing. The mixing fan speed was varied by varying the applied voltage for experiments with a single CO gas concentration of 95 mg/m^3. These data are shown in Figure 15 which shows that the sensor response time achieved a minimum of approximately 10-12 s for voltage settings greater than about 6 V. A fan voltage of 12 volts was used for all subsequent tests.

Table 3: Figaro TGS5042 Response times without fan

CO Concentration (mg/m^3)	*Average Response Time (s)*	*Standard Deviation of Response Time (s)*
20	32.9	18.2
60	60.3	53.0
80	41.9	34.6
300	40.8	17.1
900	70.3	57.2

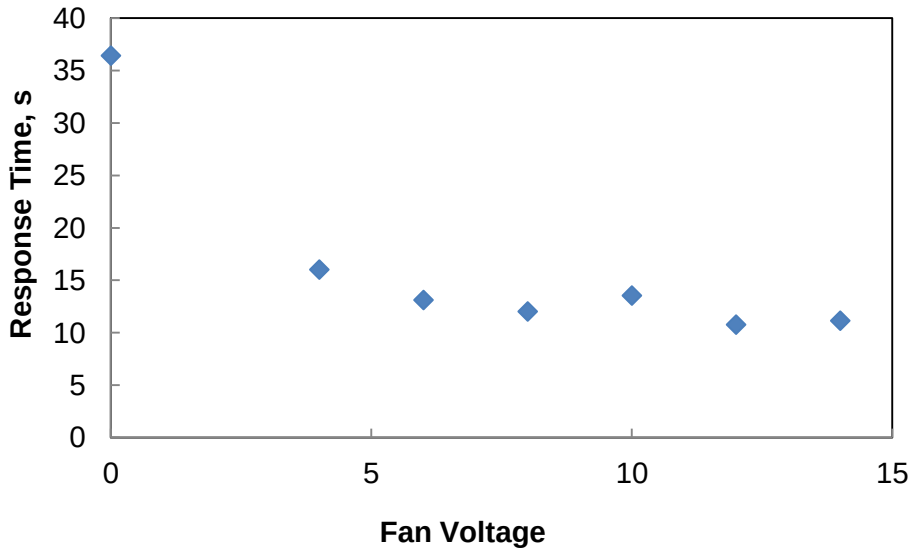

Figure 15: Mean response time shown as a function of fan voltage. Three tests were conducted at 95 mg/m^3 CO for each fan voltage

3.3 Sensor Experiments

Experiments were conducted to determine the steady state accuracy of the sensors and the transient response characteristics such as response time. The TGS5042 and EC4-500-CO were tested concurrently. The CO-B4 was tested separately because of the concentration range difference between the CO-B4 and the other two sensors.

The concentration of CO in the transient response test chamber was calculated as follows. The volume of the bladder was determined using the imposed flow rate from the flowmeter and the time of fill. The time of fill was determined from the pressure sensor data. The pressure increased slightly in the line when the bladder fill began and decreased again when the gas fill was ended. A typical experimental data set is shown in Figure 16.

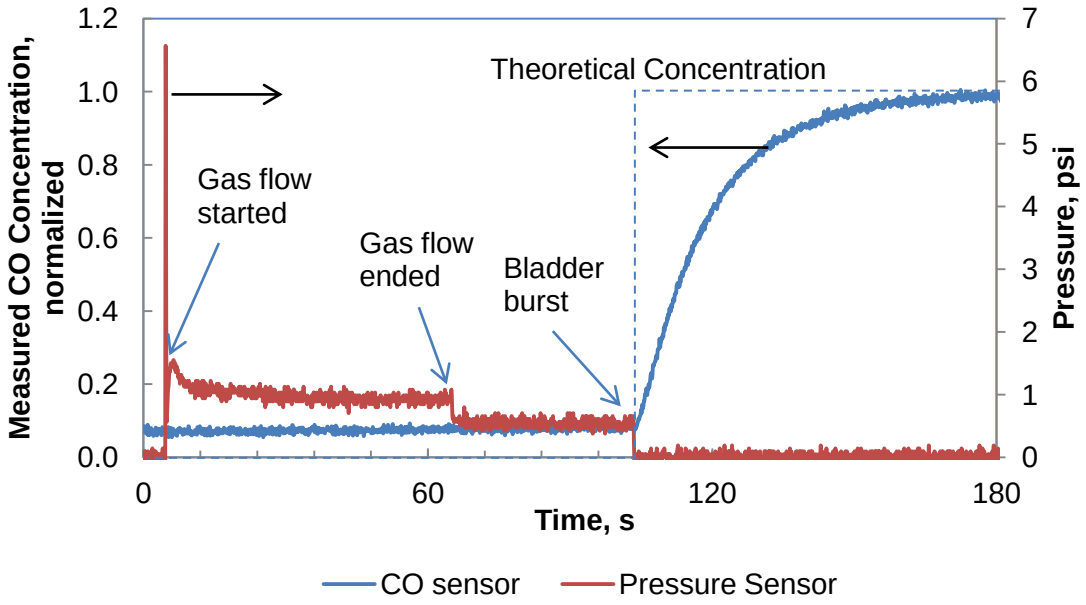

Figure 16: Typical sensor experiment with the pressure transducer data shown in red and the normalized sensor data shown in blue. The theoretical concentration of the chamber is shown in the dashed line. The gas flow start, end and bladder burst points are labeled on the pressure transducer curve.

Because the bladder does not completely fill the volume of the test chamber the concentration in the test chamber is diluted compared to the gas concentration used to fill the bladder. The actual mean gas concentration in the transient response chamber after bladder rupture was calculated as Equation (4).

$$C = \frac{F_g t C_0}{V} \tag{4}$$

Here C is the concentration in the test chamber, F_g is the mean flow rate of the test gas, t is the fill time, C_0 is the concentration of the gas supplied to the bladder, and V is the overall chamber volume.

A small amount of oxygen is necessary in the electrochemical reaction used by these sensors to detect CO [18], [21]. The premixed tanks provided by Airgas Inc. were a specified concentration of CO with a balance of N_2. With no oxygen in the premixed gas tanks the oxygen must be provided elsewhere. The chamber volume not filled by the bladder contained normal lab air. This air does not contain CO so it does not change the absolute amount of CO in the chamber, but it does contain approximately 21% oxygen. The volume of the bladder is approximately half of the total chamber volume. This results in an almost 50% dilution of CO concentration from the bladder to the chamber, and it also results in about 10% oxygen being left in the chamber. This level of oxygen is more than adequate for reliable sensor operation.

The steady state response of the sensors was tested over a range of concentrations. The TGS5042 and EC4-500-CO were tested at concentrations of 10, 30, 60, 90, and 145 mg/m^3 CO. The CO-B4 was tested at concentrations of 1, 5, and 10 mg/m^3 CO. The Figaro TGS5042 sensor was also tested at room temperature (70 °F), 100 ºF, and 120 °F.

3.4 Data Acquisition

Each sensor was connected to a manufacturer supplied evaluation board. The Figaro TGS5042 sensor was connected to a COM5042 evaluation board. The COM5042 outputs a voltage (1-9 V) that linearly varies with concentration. Each TGS5042 is stamped with a calibration from the manufacturer showing the sensitivity in nA/ppm. The manufacturers' calibration was performed using 300 ppm CO. The voltage output from the COM5042 was converted to a current using Eq. (5).

$$I_s = \frac{(\mathcal{E}_{out} - 1)}{3.13} \quad (5)$$

In this equation I_s, is the output current and $\mathcal{E}_{out}$ is the output voltage. The current is then converted to a concentration using the sensitivity of the particular sensor [21].

The e2v EC4-CO-500 sensor was connected to an ECQV-EK3 evaluation board. The ECQV-EK3 has several settings in the custom software provided with the board that can be changed to customize the output of the sensor. The manufacturer requires that the user first calibrate the sensor/evaluation board system by providing exposure to a zero CO gas as well as a calibration gas (i.e., "span" gas). This gives sensitivity in nA/ppm. Software built into the ECQV-EK3 board then outputs the appropriate concentration as the sensor responds to an applied gas. The software can also be configured to have the ECQV-EK3 output an analog voltage. This feature was used as a voltage input to the data acquisition system in the current investigation. One drawback of the e2v software was that it only outputs a value every second due to the averaging routine built in the internal software before the signal is sent through the analog output [23].

The Alphasense CO-B4 sensor is factory mounted to an evaluation board and calibrated by the manufacturer at the factory. Because of the extreme sensitivity of the sensor the manufacturer does not recommended recalibrating or uncoupling the sensor from the evaluation board unless high precision gas concentrations are available for user recalibration. The CO-B4 is a 4 electrode sensor where the others have only 3 electrodes. With the 4 electrode arrangement the sensor outputs signals from a working electrode and an auxiliary electrode. Both the auxiliary and working electrodes are corrected for a zero offset by subtracting the zero value for each electrode from the signal. The auxiliary

electrode is then used to correct the working electrode for offset drift by subtracting the auxiliary electrode signal from the working electrode signal. The corrected signal is then multiplied by the manufacturer supplied sensitivity to get the concentration of CO [20].

Once the signal from the sensor itself goes through the evaluation board the analog signals were then passed to a DI-158 USB-based data acquisition module from DataQ Instruments, Akron, OH. Sensor data were acquired at 10 Hz and written to a Microsoft Excel file for subsequent processing.

4. Results and Discussion

4.1 Steady State Results

4.1.1 Figaro TGS5042

The experimentally determined data for the TGS5042 sensor (acquired in the small chamber) are compared with the manufacturer's calibration (black line) in Figure 17. The experimental data exhibits a greater sensitivity (i.e., higher slope) than the calibration recommended by the manufacturer.

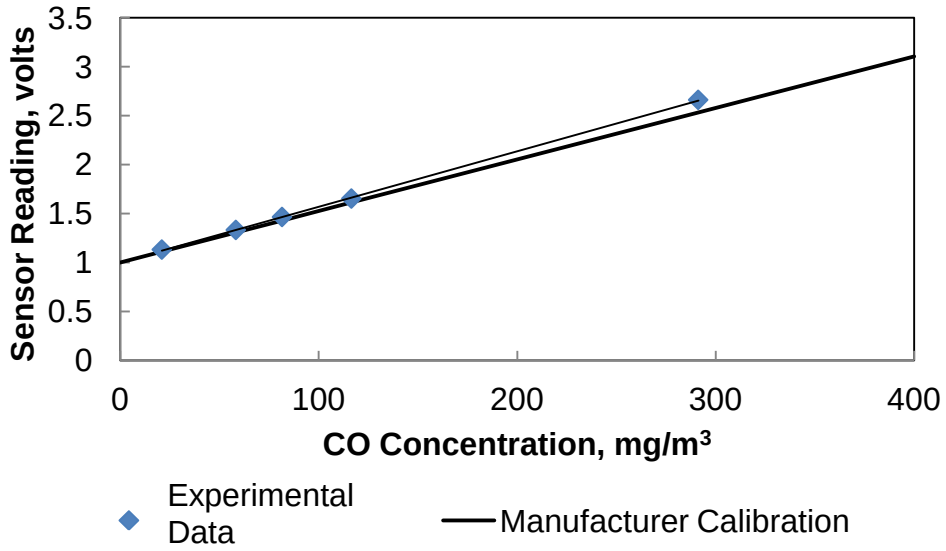

Figure 17: Figaro TGS5042 experimental data. The manufacturer calibration shown as a solid line and the current results marked by diamond symbols.

The data for Figure 17 were reversed to treat voltage as the independent variable so that the results could be used directly to convert experimental sensor voltages to CO gas concentrations. Equation (6) is the resulting linear fit to the experimental data.

$$C_{CO}\left(\frac{mg}{m^3}\right) = 176.06\mathcal{E}(Volt) - 176.3 \tag{6}$$

The best fit CO concentration predictions from Eq. (6) were applied to the steady state sensor readings from the transient bladder burst experiments and are shown in Table 4. The percent difference in the actual concentrations and predicted values from Equation (6) is also shown in Table 4. In general the TGS5042 overestimates the concentration in the test chamber. The largest differences occur at lower concentrations. The full scale range of the TGS5042 device is from 0-10,000 ppm (11,650 mg/m^3) and the signal-to-noise ratio is low at concentrations less than 50 mg/m^3. This low signal-to-noise ratio results in the larger errors exhibited at the lowest concentrations.

Table 4: Figaro TGS5042 steady state results

CO Concentration (mg/m^3)	*CO Prediction from Eq. 6 (mg/m^3)*	*% Difference*
10.5	14.5	39.0
30	31.0	4.7
60	61.5	3.9
90	87.1	3.2
145	146.4	1.7

* Steady state results were measured at the end of the transient bladder rupture experiments

4.1.2 e2v EC4-500-CO

The experimentally determined e2v EC4-500-CO data (acquired in the small chamber) are shown in Figure 18. As noted previously, this sensor requires an initial calibration by the user by exposing the sensor to a single known concentration of CO as well as air with no CO present and the e2v's internal software determines the appropriate calibration. The initial calibration was performed by exposing the sensor to air without CO gas as well as air with 100 ppm or 116.5 mg/cm^3 CO. The internal calibration is shown in Figure 18 as the open symbol. The sensor was then exposed to three other certified gas concentrations as shown in Figure 18 and a separate linear fit was then applied to the data. Equation (7) shows the experimental fit to the four certified gas concentrations.

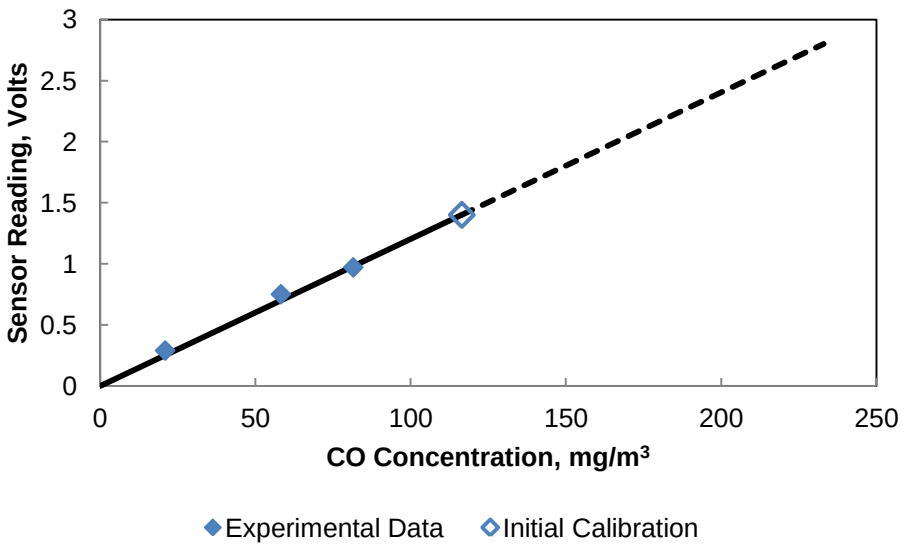

Figure 18: e2v EC4-500-CO calibration curves. The manufacturer calibration shown as a solid line and the current results marked by diamond symbols.

Note that the predicted line goes through zero without an experimental offset as seen previously with the Figaro sensor.

$$C_{CO}\left(\frac{mg}{m^3}\right) = 79.861\mathcal{E}(Volts) \tag{7}$$

The best fit CO concentration predictions from Eq. (7) were applied to the steady state sensor readings from the transient bladder burst experiments and are shown in Table 5. The largest percent differences between the certified gas concentrations and the predictions of Eq. (7) are seen at the lowest concentration where the signal-to-noise ratio is also lowest.

Table 5: e2v EC4-500-CO steady state results

CO Concentration (mg/m^3)	*CO Prediction from Eq. 7 (mg/m^3)*	*% Difference*
10.5	13.2	26.3
30	31.8	7.5
60	65.2	10.2
90	88.5	1.7
145	155.3	7.1

* Steady state results were measured at the end of the transient bladder rupture experiments

4.1.3 Alphasense CO-B4

The Alphasense CO-B4 sensor has the highest sensitivity of the three sensors investigated and the manufacturer's calibration was used for all experiments done with the CO-B4. The steady state results are shown in Table 6. The sensor responds linearly to

an increase in CO concentration. The sensor consistently overestimates the concentration of CO, and the percent error is larger than the other sensors. The CO-B4 is precise and the standard deviation between the different runs is very low.

Table 6: Alphasense CO-B4 steady state results

CO Concentration (mg/m^3)	*Sensor CO Reading (mg/m^3)*	*Standard Deviation (mg/m^3)*	*% Error*
1.2	1.6	0.07	34.0
5	6.3	0.02	22.7
10	11.8	0.21	17.2

* Steady state results were measured at the end of the transient bladder rupture experiments

The steady state experimental results for the Alphasense CO-B4 sensor are shown in Figure 19. The vertical bars show the uncertainty in the sensor reading, and the horizontal bars show the uncertainty in the CO concentration in the chamber due to uncertainty in the volume of the chamber.

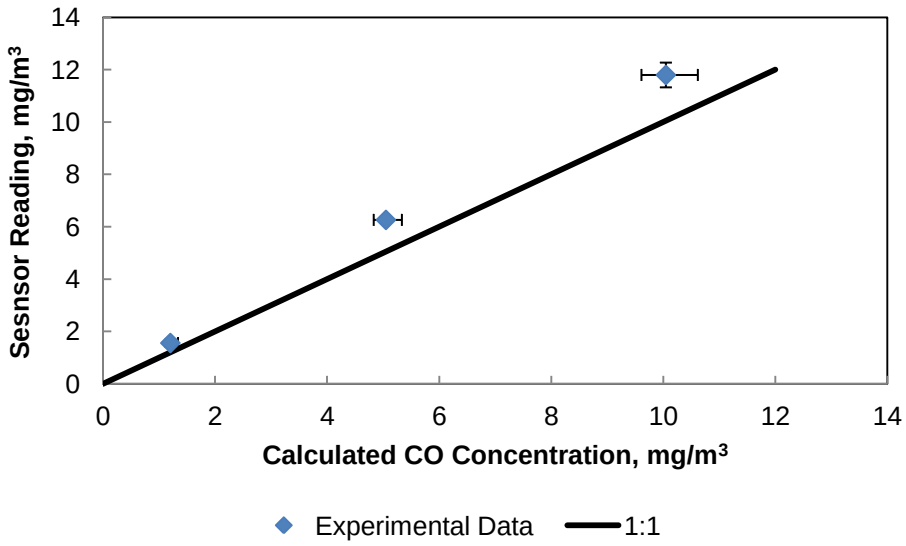

Figure 19: Alphasense CO-B4 experimental data. The bars show the uncertainty in the calculated concentration and the sensor reading. The solid line shows a 1:1 relationship.

4.1.4 Steady State Comparison

The steady state responses of all three sensors are shown in Figure 20. The solid line indicates a 1:1 ratio where the sensor reading would be equal to the actual concentration. All three sensors lie very close to the 1:1 relationship.

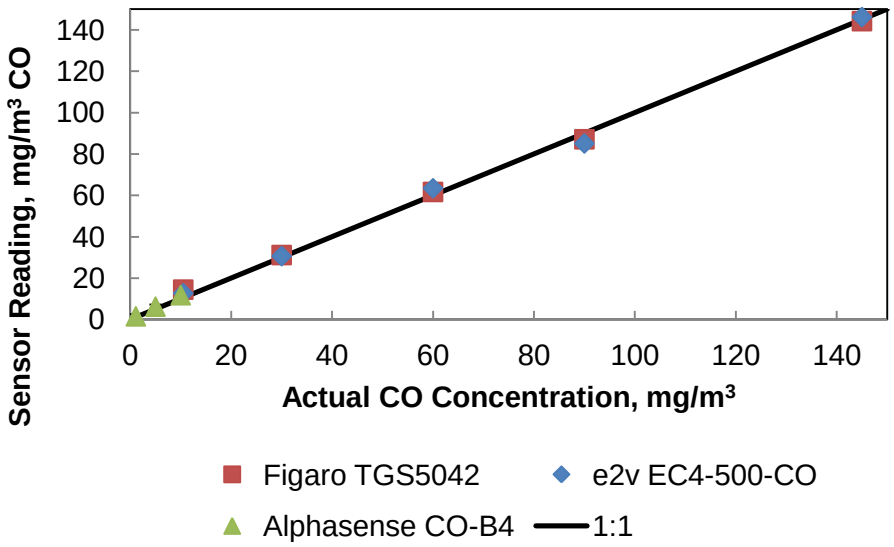

Figure 20: Steady state comparison of the CO-B4 (triangles), Figaro TGS5042 (squares), and e2v EC4-500-CO (circles). The sensor readings were compared with the actual concentration and the ideal 1:1 relationship (solid).

The sensors' response to temperature changes is also of interest. The electrochemical reaction that occurs inside an electrochemical CO sensor can be affected by temperature changes. Both the e2v EC4-500-CO and the Figaro TGS5042 have thermistors that compensate the sensors' output for the actual temperature. The results from the Figaro TGS5042 are shown in Figure 21. The slopes of the response for 70º F (room temperature), 100º F and 120º F are all equal indicating that temperature compensation has occurred on the sensor evaluation board.

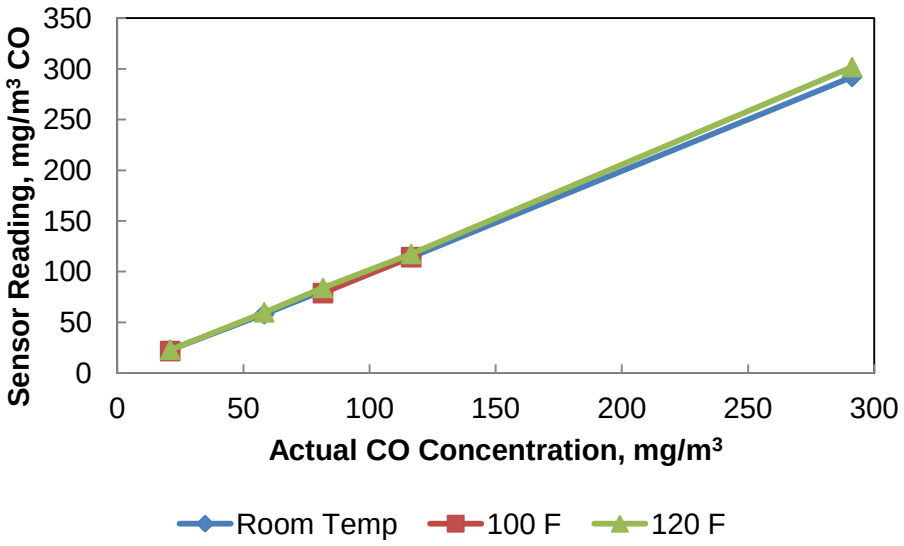

Figure 21: Figaro TGS5042 sensor reading compared with the actual concentration for room temperature, 100 ºF, and 120 °F.

4.2 Transient Results

The transient response of each sensor was characterized by experimentally determining the response time for each sensor. The response times given are the times from the initial gas release due to bladder rupture to when the sensor reaches 90% of the final steady state concentration. The transient response was also characterized by the time to detection. The RMS noise for each sensor was quantified before any exposure to CO. The time to event detection was defined as the time to reach 3 times the zero gas RMS noise. Three times the RMS noise is a standard limit of detection in analytical chemistry [24]. The rate of sensor response at the time to event detection was also calculated for the TGS5042 sensor and the EC4-500-CO sensor. The rate of sensor response was found using a linear curve fit in Microsoft Excel.

4.2.1 Figaro TGS5042

The response times for the TGS5042 are shown in Table 7.The response times across concentrations are consistent with an average response time of 11.5 seconds to reach 90% of the final steady state value of the sensor response. However, the time to event detection varies with the concentration level associated with each event. The lowest concentration level events take the longest times to reliably detect that an event has occurred. The low signal-to-noise ratio leads to higher times to detection since three times the RMS noise is a significant proportion of the final steady state value when concentrations are low. An increase in CO concentration leads to a decrease in time to detection. The reason for this can be seen in Figure 22. The sensor responses to 30, 90, and 145 mg/m^3 CO are shown. The slope of the response curve immediately after each event increases with increasing concentration. Since the response time stays constant across different concentrations of CO, the slope of the response in $\frac{mg/m^3}{s}$ must increase with increasing concentration.

Figure 23 shows the Figaro TGS5042 sensor response curves normalized with respect to the final concentrations (i.e., C/C_{final}) for the exposures to 30, 90, and 145 mg/m^3 CO. The normalized response curves overlay one another as expected.

Table 7: Figaro TGS5042 transient response times

Concentration (mg/m^3)	*Response Time t_{90} (s)*	*Time to Event Detection (s)*
10.5	10.0	5.4
30	12.9	2.8
60	11.0	1.8
90	12.1	1.3
145	11.4	0.8
Mean	*11.5*	*2.4*

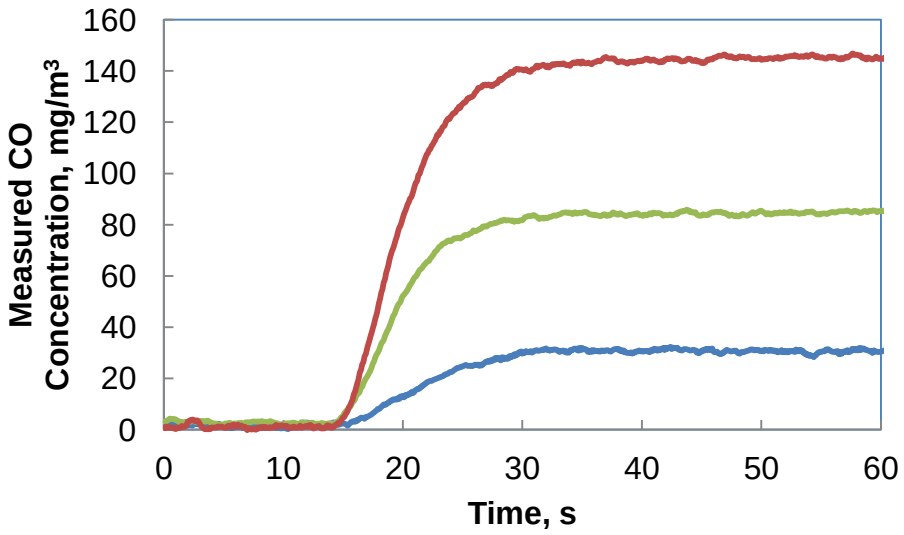

Figure 22: Figaro TGS5042 sensor response for 30, 90 and 145 mg/m^3 CO

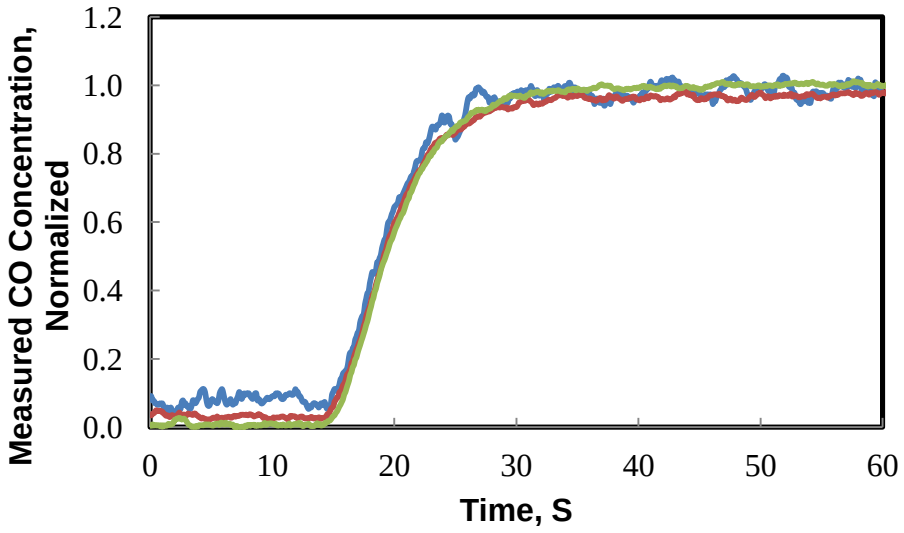

Figure 23: Figaro TGS5042 sensor response to 30, 90, and 145 mg/m^3 CO normalized by the final steady state value.

The rate of response of the Figaro TGS5042 sensor to the instantaneous exposure to CO is plotted against gas concentration in Figure 24. Interestingly, the rate of sensor response increases linearly with concentration over the range of concentrations examined.

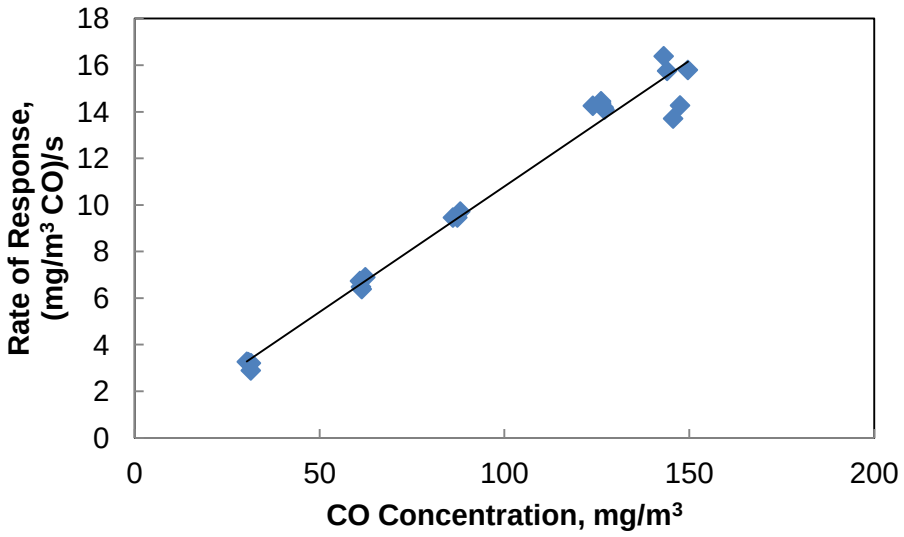

Figure 24: Figaro TGS5042 rate of response vs. concentration. A linear curve fit is shown as a solid line.

4.2.2 e2v EC4-500-CO

The response times and the times to event detection for the e2v EC4-500-CO sensor are shown in Table 8. The mean response time exhibited by this sensor is slightly longer than that exhibited by the Figaro TGS5042. The e2v evaluation board contains onboard averaging while the evaluation board for the Figaro sensor does not. The e2v ECVQ-EK3 averages values over 1 second and updates the output through the analog output only once a second. This leads to wider variation in the response times since the value is only updated once a second. Interestingly, the mean time to event detection of

the e2v EC4-500-CO sensor was less than the Figaro TGS5043 sensor (1.4 s vs. 2.4 s, respectively).

Table 8: e2v EC4-500-CO transient response times

CO Concentration (mg/m^3)	*Response Time t_{90} (s)*	*Time to Event Detection (s)*
10.5	12.5	2.0
30	18.6	1.3
60	11.2	1.4
90	16.7	1.0
145	12.5	1.0
Mean	*14.3*	*1.4*

The rate of sensor response for the e2v EC4-500-CO sensor to the instantaneous exposure to CO is shown in Figure 25. The scatter in the data here is larger than for the Figaro TGS5042, presumably because of the averaging algorithm of the evaluation board output.

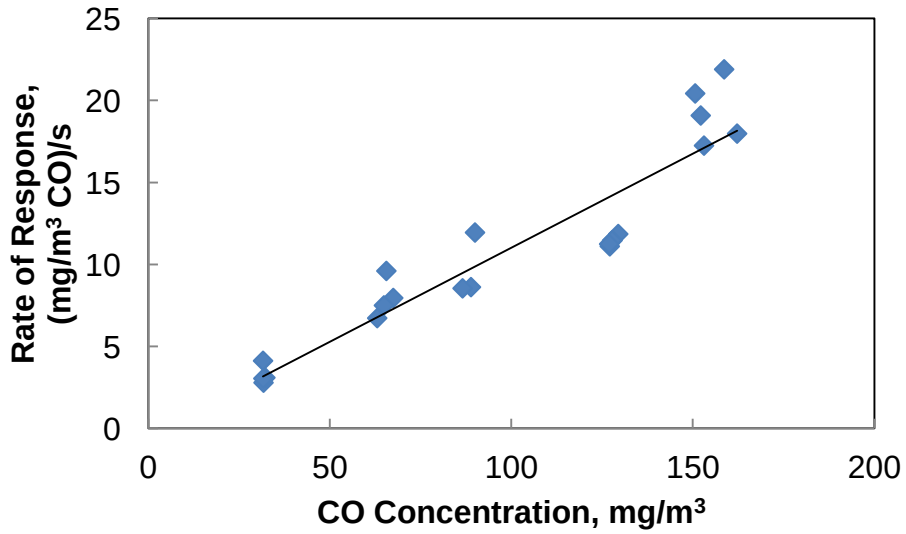

Figure 25: e2v EC4-500-CO rate of response vs. concentration. A linear curve fit is shown as a solid line.

4.2.3 Figaro TGS5042 and e2v EC4-500-CO Response Comparison

The rates of sensor response were also compared in two different test chambers to ensure the sensor response rates were intrinsic characteristics of the sensors themselves and not affected by the test chamber. Transient experiments with the Figaro TGS5042 sensor using the bladder burst technique were conducted in the smaller chamber (volume of 2.5L) for comparison with the data from the larger chamber (volume of 16.7L). The sensor response rates for the EC4-500-CO sensor determined in the large chamber are also included for comparison. The rates of sensor response for both sensors exhibit the same dependency upon exposure concentration regardless of chamber size. Thus, the sensor response rates appear to be intrinsic to the sensors themselves and likely due to similar gaseous diffusion kinetics for the two sensors.

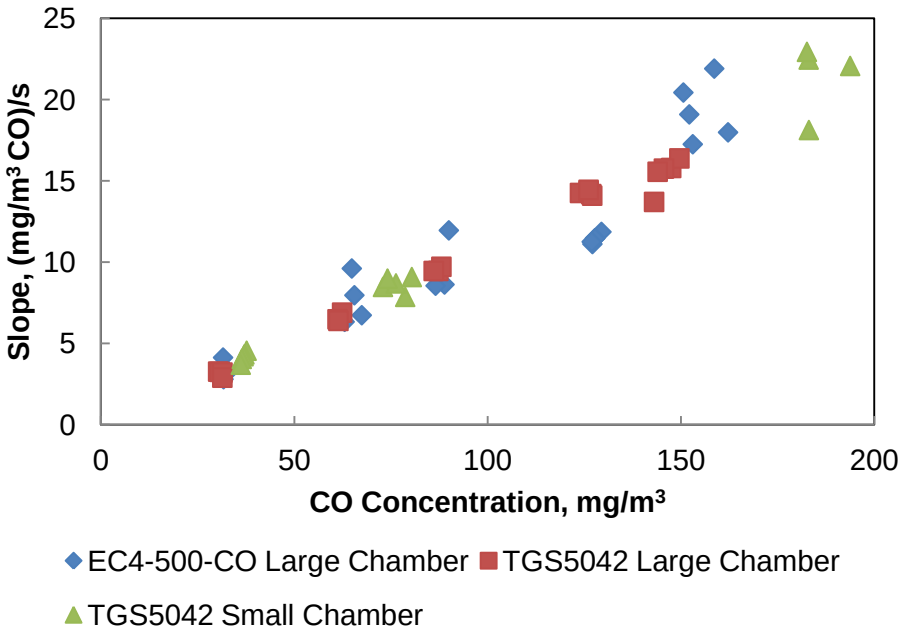

Figure 26: Comparison of rate of response of TGS5042 in large and small chambers. EC4-500-CO rate of response for the large chamber is also shown.

4.2.4 Potential for Using the Sensor Rate of Response to Estimate Final Steady State Values

Since the sensors' rates of response change predictably with CO concentration as shown in Figure 24 –Figure 26, the rates of response when each sensor reaches the detection limit, designated as 3 times the RMS noise, can be used to estimate the final steady state value before the sensor actually reaches steady state. This allows an estimate of the CO concentration in less time than required while waiting for the sensor to equilibrate. This procedure was tested by exposing a Figaro TGS5042 sensor to 61.5 mg/m^3 CO and acquiring data for 2 seconds (20 data points) after the sensor reached the limit of detection. These data are shown in Figure 27. The response rate thus determined ($5.38 \frac{mg/m^3}{s}$) was then used with the data shown in Figure 26 to estimate the final steady state concentration. A concentration of 59.6 mg/m^3 CO was estimated which is only 3.1% less than the actual exposure concentration. The Figaro TGS5042 reached a steady state concentration reading of 61.2 mg/m^3 which is 0.5% less than the actual exposure concentration.

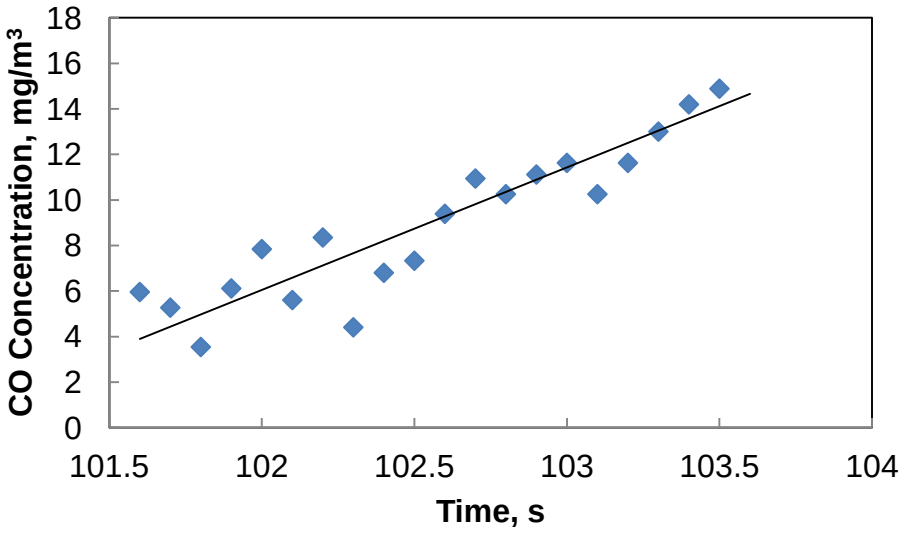

Figure 27: A Figaro TGS5042 was exposed to 61.5 mg/m^3 CO and the response is shown for 2 seconds starting at the time of detection. The solid line is a linear curve fit used to determine the rate of response.

4.2.5 Very Low Level Sensing Using the Alphasense CO-B4

The Alphasense CO-B4 sensor is designed to measure very low levels of CO concentration. The transient response times and times to detect an event for this sensor are shown in Table 9. The response times for the CO-B4 are 2 to 3 times higher than the response times for the Figaro TGS5042 and the e2v EC4-500-CO. But, the time to event detection is of the same order as the time to event detection for the other sensors presumably because of the low noise of the CO-B4 technology.

Also, and unlike the other two sensors, the response time of the Alphasense CO-B4 sensor was dependent on CO concentration. The CO-B4 takes considerably longer to achieve a steady state value with a higher concentration of CO.

Table 9: Alphasense CO-B4 transient response times

CO Concentration (mg/m^3)	*Response Time t_{90} (s)*	*Time to Detection (s)*
1.2	30.2	3.2
5	34.2	2.8
10	37.1	0.5
Average	*33.8*	*2.2*

5. Conclusions

Three commercial, electrochemical CO sensors were purchased and the steady state and transient response of each was examined. The e2v EC4-500-CO and the Figaro TGS5042 are comparable sensors designed for use in homes or industrial detection of CO concentrations. The Alphasense CO-B4 is a sensor specially designed to detect low concentrations of CO. All three sensors were tested using a chamber designed to provide a step concentration change of CO. The steady state accuracy as well as the transient response and response times were reported for each sensor.

The commercially available CO sensors tested were reliable and accurate, and the sensors all had relatively quick response times. The Figaro TGS and e2v EC4-500-CO had response times of 11 seconds and 14 seconds respectively while the Alphasense CO-B4 had a response time of 34 seconds. The signal from all three sensors increased linearly with increasing CO concentrations. The transient response of the Figaro TGS5042 allows for prediction of the steady state CO concentration after only a few seconds. This could be very valuable in situations where the concentration changes rapidly and the system does not reach steady state. The e2v EC4-500-CO sensor could also be used for this purpose, but the software used to control the ECVQ-EK3 would need to be modified to update the output values more than once a second. A whole new electronics package could also be developed to process the sensor output. Though the CO-B4 had a longer response time, the sensor is able to detect very low CO concentrations. In this study

concentrations as low as 1 mg/m^3 CO were measured. The ability to detect small CO concentrations could prove very valuable in the bleed air system due to the high dilution rates of any fumes entering the air stream.

Commercially available CO sensor technology is mature and would work well for monitoring the bleed air conditions of an airliner. The Figaro TGS5042 and e2v EC40-500-CO are able to respond quickly and accurately to a change in CO concentration. The CO-B4, though slower responding, is able to detect small concentrations of CO. Combining these sensors into a package to monitor the air quality in an airliner would provide very useful information.

6. Future Work

The three electrochemical sensors evaluated in this work performed well under laboratory circumstances. These sensors need to be evaluated in a more real environment with gas mixtures that include other gases than CO and N_2 to ensure the sensors work properly in the presence of other gases. The next step to evaluate the sensors is to use them to evaluate the bleed air system of an aircraft. The Vehicle Integrated Propulsion Research (VIPR) program aims to contaminate the bleed air system with engine oil and then measure the evolved gases that pass through the bleed air system. Eventually the goal is to use commercially available CO sensors such as the ones examined in this study to monitor the air quality in the airline cabin.

7. References

[1] Lufthansa Technik, “Breathing at High Altitude: The air supply of aircraft cabins.” [Online]. Available: http://www.lufthansa-technik.com/cabin-air-circulation.

[2] J. Spengler and D. Wilson, “Air quality in aircraft,” *Proc. Inst. Mech. Eng.*, vol. 217, no. Part E: J. Process Mechanical Engineers, Nov. 2003.

[3] S. Nassauer, “Up in the Air: New Worries About ‘Fume Events’ on Planes,” *The Wall Street Journal*, 30-Jul-2009. [Online]. Available: http://online.wsj.com/news/articles/SB10001424052970204900904574302293012711628.

[4] J. Gold, “Boeing suit settlement stirs jetliner air safety debate,” *MSNBC News*, 06-Oct-2011. [Online]. Available: http://www.nbcnews.com/id/44777304/ns/travel-news/#.UoJ0s_l69Wj.

[5] M. Dechow and C. A. H. Nurcombe, “Aircraft Environmental Control Systems,” *Hdb Env Chem*, vol. 4, no. Part H, pp. 3–24, 2005.

[6] C. van Netten and V. Leung, “Comparison of the Constituents of Two Jet Engine Lubricating Oils and Their Volatile Pyrolytic Degradation Products.,” *Appl. Occup. Environ. Hyg.*, vol. 15, no. 3, pp. 277–283, Mar. 2000.

[7] J. Anderson, *Introduction to Flight*, 6th ed. McGraw Hill Higher Education, 2008.

[8] E. Hunt, D. Reid, D. Space, and F. Tilton, “Commercial Airliner Environmental Control System: Engineering Aspects of Cabin Air Quality,” presented at the Aerospace Medical Association Annual Meeting, Anaheim, CA, 1995.

[9] J. Murawski, “Occupational and Public Health Risks,” *Hdb Env Chem*, vol. 4, Part H, pp. 25–51, 2005.

[10] R. Haney, “Principle Component Analysis for Enhancement of Infrared Spectra Monitoring,” Doctoral Disertation, Auburn University, 2011.

[11] CDC, “Cabon Monoxide Poisoning.” Department of Health and Human Services.

[12] “Carbon Monoxide Questions and Answers,” *United States Consumer Product Safety Commission*. [Online]. Available: http://www.cpsc.gov/en/Safety-Education/Safety-Education-Centers/Carbon-Monoxide-Information-Center/Carbon-Monoxide-Questions-and-Answers-/.

[13] “C.F.R. § 25.831 (2013).” .

[14] “29 CFR Table Z-1.” .

[15] “ACGIH 1994, p. 15.” .

[16] “NIOSH 1992.” .

[17] R. Knake, P. Jacquinot, A. W. E. Hodgson, and P. C. Hauser, “Amperometric sensing in the gas-phase.,” *Anal. Chim. Acta*, vol. 549, no. 1/2, pp. 1–9, Sep. 2005.

[18] “How Electrochemical Gas Sensors Work.” Alphasense Ltd.

[19] I. Helm, L. Jalukse, and I. Leito, “Measurement Uncertainty Estimation in Amperometric Sensors: A Tutorial Review.,” *Sens. 14248220*, vol. 10, no. 2, pp. 4430–4455, Feb. 2010.
[20] “Alphasense 4-Electrode Individual Sensor Board (ISB) Issue 4.” Alphasense Ltd., Jun-2012.
[21] “Technical Information for TGS5042.” Figaro Inc., Dec-2007.
[22] “e2v gas sensor product overview.” e2v Technologies.
[23] “EC4-500-CO Carbon Monoxide Electrochemical Sensor.” e2v Technologies, Oct-2009.
[24] S. Ahuja and N. Jespersen, *Modern Instrumental Analysis*. Elsevier, 2006.

Appendix – I

Airgas Certificates of Analysis

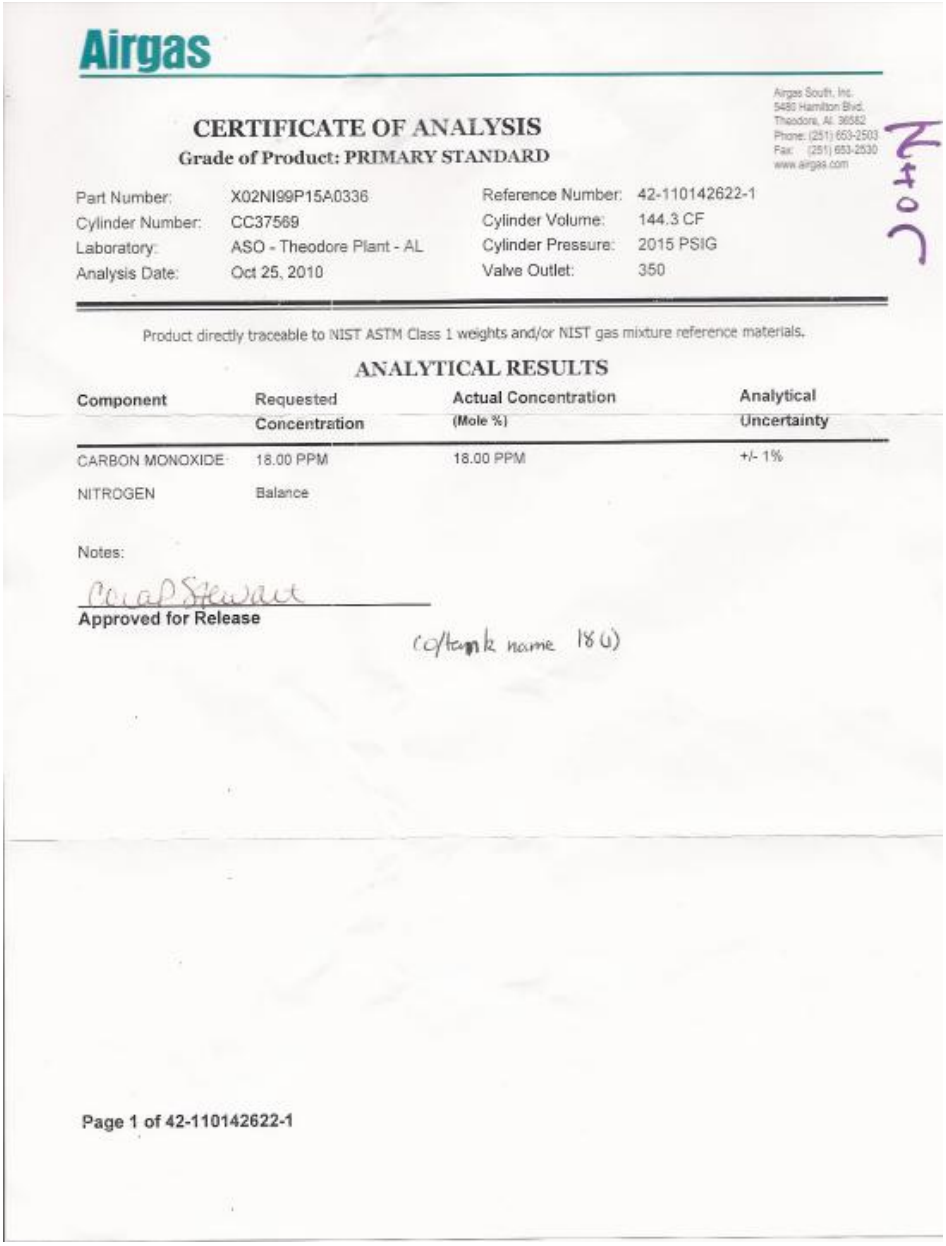

Airgas

Airgas South, Inc.
5480 Hamilton Blvd.
Theodore, Al. 36582
Phone: (251) 653-2503
Fax: (251) 653-2530
www.airgas.com

CERTIFICATE OF ANALYSIS

Grade of Product: PRIMARY STANDARD

Part Number:	X02NI99P15A0336	Reference Number:	42-110142622-1
Cylinder Number:	CC37569	Cylinder Volume:	144.3 CF
Laboratory:	ASO - Theodore Plant - AL	Cylinder Pressure:	2015 PSIG
Analysis Date:	Oct 25, 2010	Valve Outlet:	350

Product directly traceable to NIST ASTM Class 1 weights and/or NIST gas mixture reference materials.

ANALYTICAL RESULTS

Component	Requested Concentration	Actual Concentration (Mole %)	Analytical Uncertainty
CARBON MONOXIDE	18.00 PPM	18.00 PPM	+/- 1%
NITROGEN	Balance		

Notes:

Carol Stewart
Approved for Release

cc/tank name 180

Page 1 of 42-110142622-1

Figure A1: Airgas Certification of 18 ppm CO

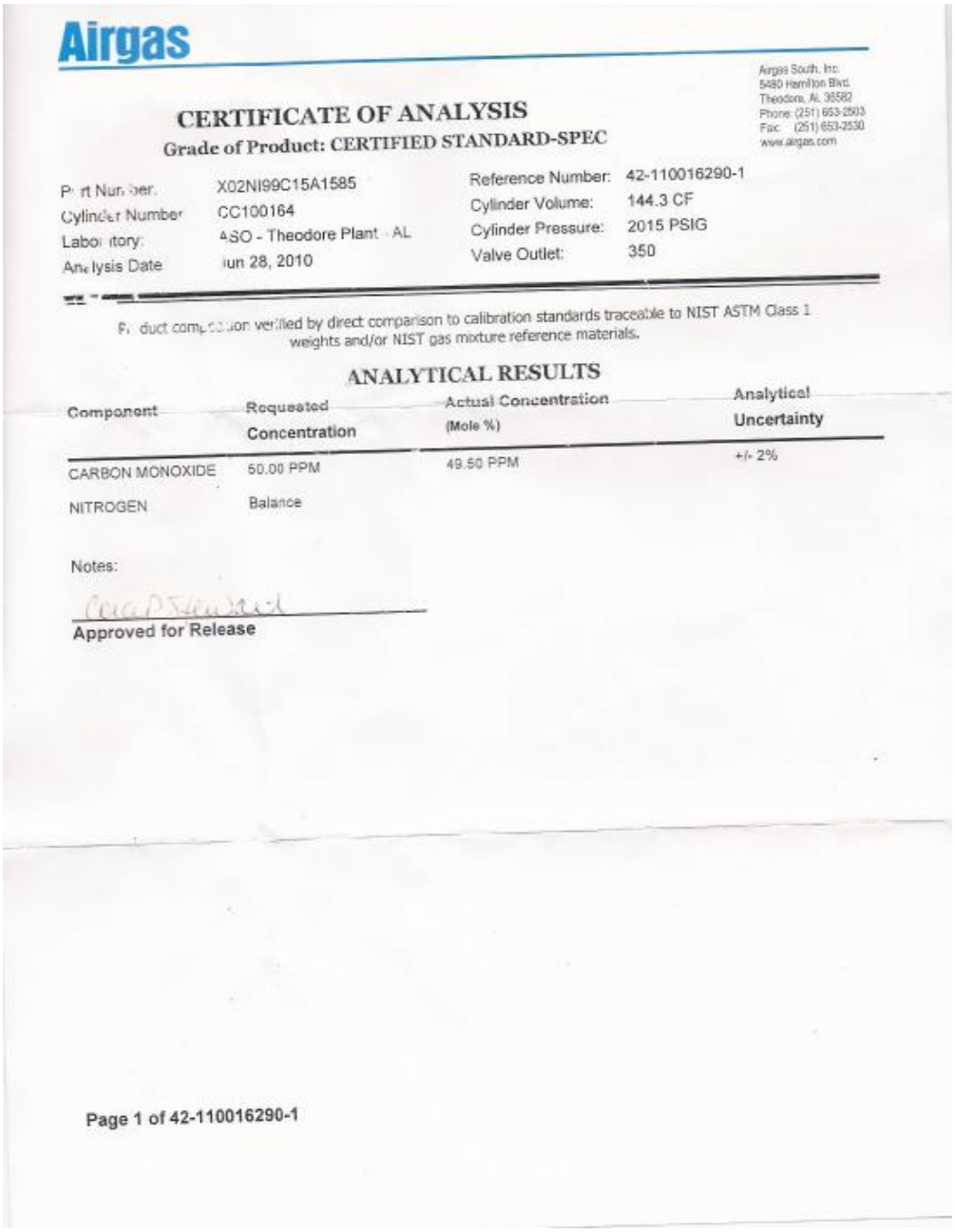

Airgas

Airgas South, Inc.
5480 Hamilton Blvd.
Theodore, AL 36582
Phone: (251) 653-2503
Fax: (251) 653-2530
www.airgas.com

CERTIFICATE OF ANALYSIS

Grade of Product: CERTIFIED STANDARD-SPEC

Part Number:	X02NI99C15A1585	Reference Number:	42-110016290-1
Cylinder Number:	CC100164	Cylinder Volume:	144.3 CF
Laboratory:	ASO - Theodore Plant - AL	Cylinder Pressure:	2015 PSIG
Analysis Date:	Jun 28, 2010	Valve Outlet:	350

Product composition verified by direct comparison to calibration standards traceable to NIST ASTM Class 1 weights and/or NIST gas mixture reference materials.

ANALYTICAL RESULTS

Component	Requested Concentration	Actual Concentration (Mole %)	Analytical Uncertainty
CARBON MONOXIDE	50.00 PPM	49.50 PPM	+/- 2%
NITROGEN	Balance		

Notes:

Approved for Release

Page 1 of 42-110016290-1

Figure A2: Airgas Certification of 50 ppm CO

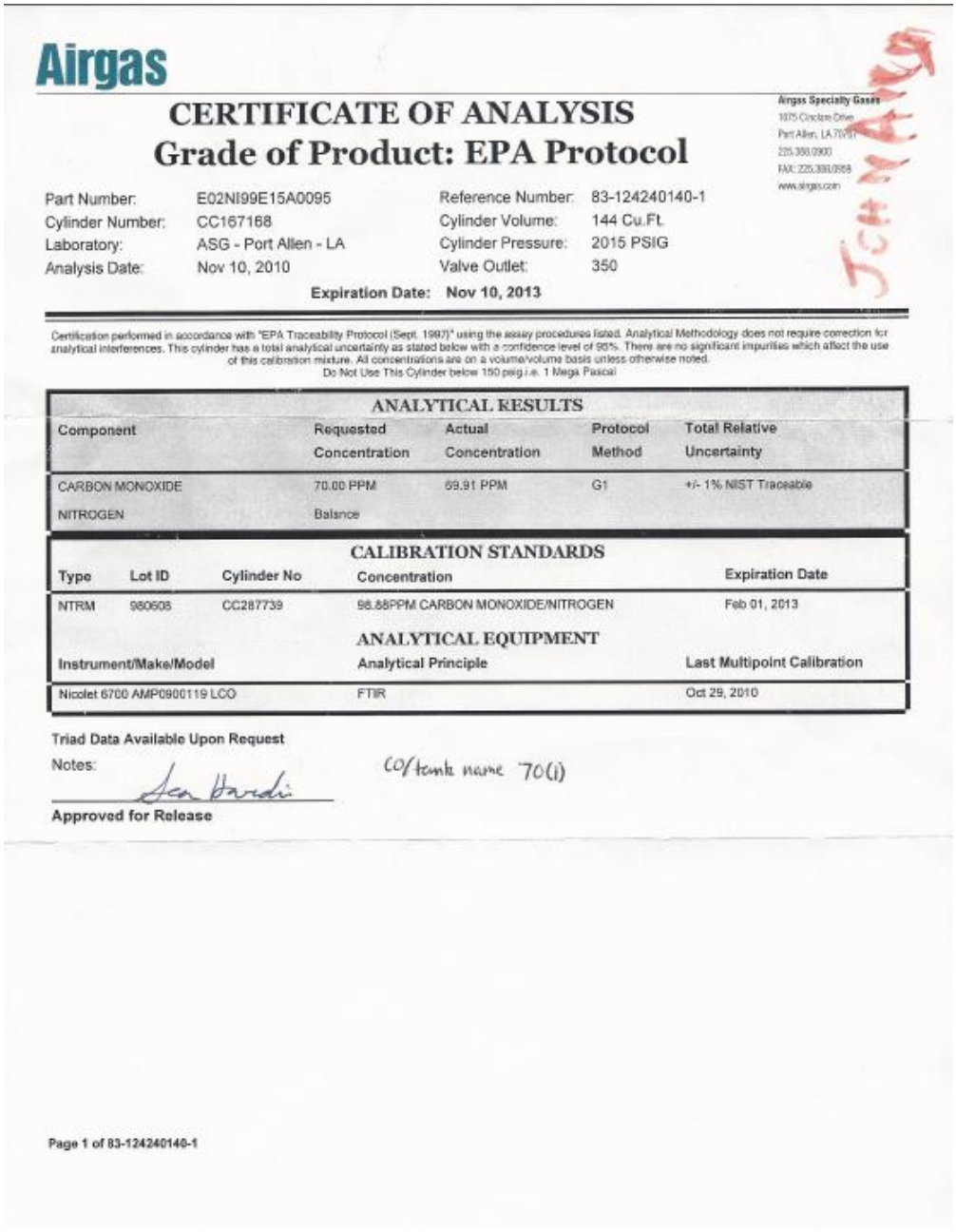

Airgas

CERTIFICATE OF ANALYSIS
Grade of Product: EPA Protocol

Airgas Specialty Gases
1075 Cinclare Drive
Port Allen, LA 70767
225.388.0900
FAX: 225.388.0958
www.airgas.com

Part Number:	E02NI99E15A0095	Reference Number:	83-124240140-1
Cylinder Number:	CC167168	Cylinder Volume:	144 Cu.Ft.
Laboratory:	ASG - Port Allen - LA	Cylinder Pressure:	2015 PSIG
Analysis Date:	Nov 10, 2010	Valve Outlet:	350

Expiration Date: Nov 10, 2013

Certification performed in accordance with "EPA Traceability Protocol (Sept. 1997)" using the assay procedures listed. Analytical Methodology does not require correction for analytical interferences. This cylinder has a total analytical uncertainty as stated below with a confidence level of 95%. There are no significant impurities which affect the use of this calibration mixture. All concentrations are on a volume/volume basis unless otherwise noted.
Do Not Use This Cylinder below 150 psig i.e. 1 Mega Pascal

ANALYTICAL RESULTS

Component	Requested Concentration	Actual Concentration	Protocol Method	Total Relative Uncertainty
CARBON MONOXIDE	70.00 PPM	69.91 PPM	G1	+/- 1% NIST Traceable
NITROGEN	Balance			

CALIBRATION STANDARDS

Type	Lot ID	Cylinder No	Concentration	Expiration Date
NTRM	980608	CC287739	98.88PPM CARBON MONOXIDE/NITROGEN	Feb 01, 2013

ANALYTICAL EQUIPMENT

Instrument/Make/Model	Analytical Principle	Last Multipoint Calibration
Nicolet 6700 AMP0900119 LCO	FTIR	Oct 29, 2010

Triad Data Available Upon Request

Notes: CO/tank name 70(i)

Approved for Release

Page 1 of 83-124240140-1

Figure A3: Airgas Certification of 70 ppm CO

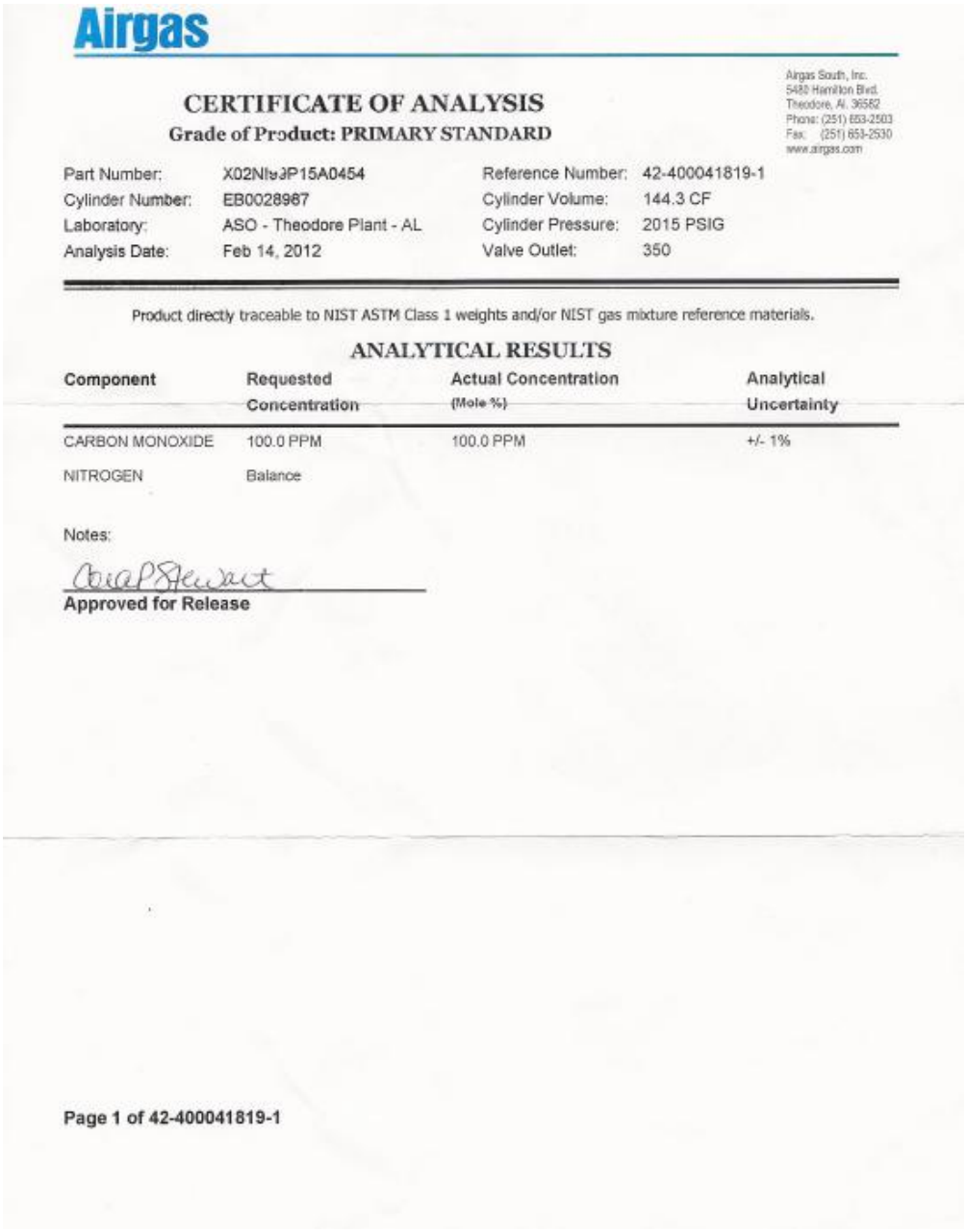

Airgas

Airgas South, Inc.
5488 Hamilton Blvd.
Theodore, Al. 36582
Phone: (251) 653-2503
Fax: (251) 653-2530
www.airgas.com

CERTIFICATE OF ANALYSIS

Grade of Product: PRIMARY STANDARD

Part Number:	X02NI9J9P15A0454	Reference Number:	42-400041819-1
Cylinder Number:	EB0028987	Cylinder Volume:	144.3 CF
Laboratory:	ASO - Theodore Plant - AL	Cylinder Pressure:	2015 PSIG
Analysis Date:	Feb 14, 2012	Valve Outlet:	350

Product directly traceable to NIST ASTM Class 1 weights and/or NIST gas mixture reference materials.

ANALYTICAL RESULTS

Component	Requested Concentration	Actual Concentration (Mole %)	Analytical Uncertainty
CARBON MONOXIDE	100.0 PPM	100.0 PPM	+/- 1%
NITROGEN	Balance		

Notes:

Approved for Release

Page 1 of 42-400041819-1

Figure A4: Airgas Certification of 100 ppm CO

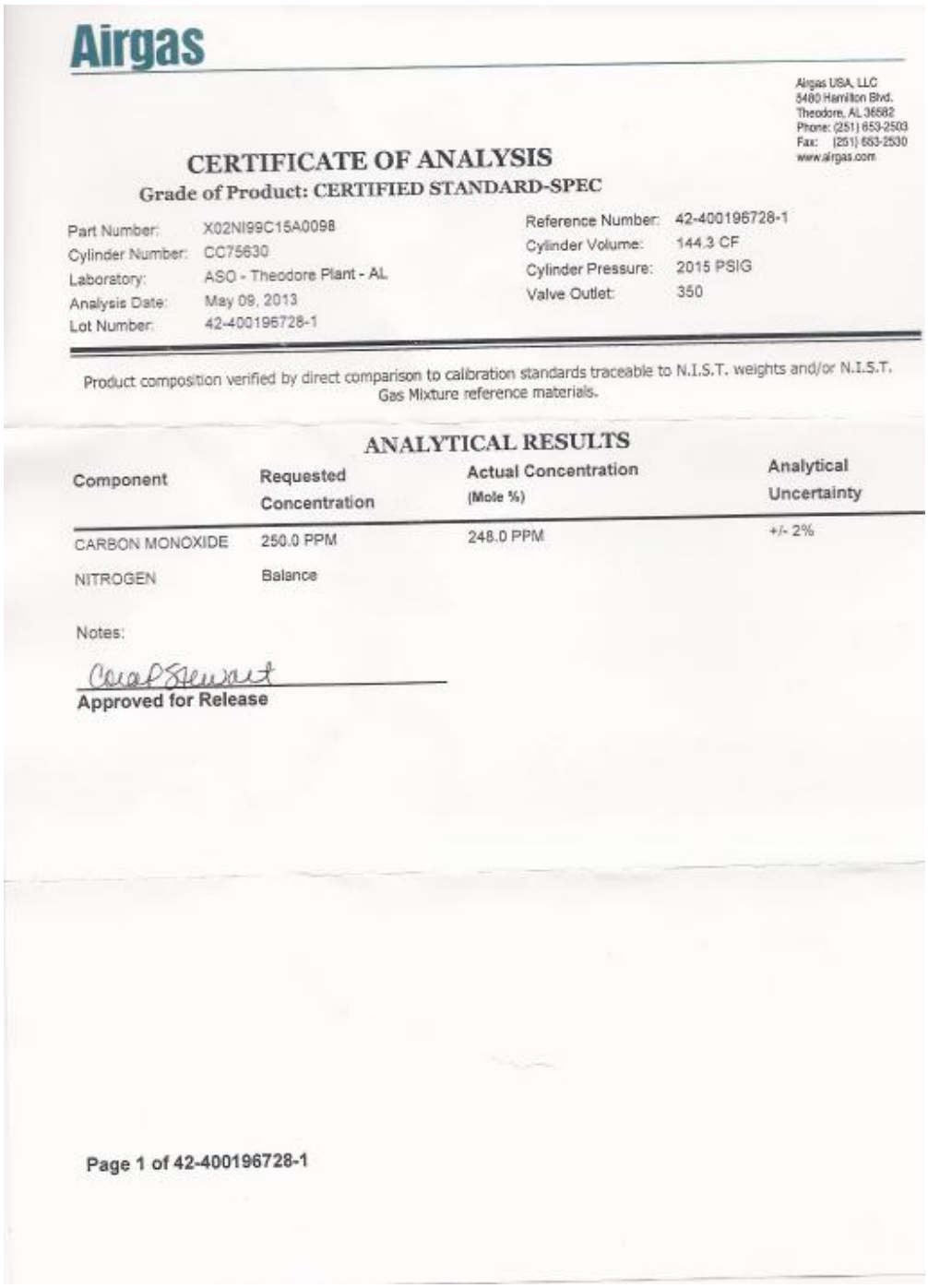

Airgas

Airgas USA, LLC
5480 Hamilton Blvd.
Theodore, AL 36582
Phone: (251) 653-2503
Fax: (251) 653-2530
www.airgas.com

CERTIFICATE OF ANALYSIS

Grade of Product: CERTIFIED STANDARD-SPEC

Part Number:	X02NI99C15A0098	Reference Number:	42-400196728-1
Cylinder Number:	CC75630	Cylinder Volume:	144.3 CF
Laboratory:	ASO - Theodore Plant - AL	Cylinder Pressure:	2015 PSIG
Analysis Date:	May 09, 2013	Valve Outlet:	350
Lot Number:	42-400196728-1		

Product composition verified by direct comparison to calibration standards traceable to N.I.S.T. weights and/or N.I.S.T. Gas Mixture reference materials.

ANALYTICAL RESULTS

Component	Requested Concentration	Actual Concentration (Mole %)	Analytical Uncertainty
CARBON MONOXIDE	250.0 PPM	248.0 PPM	+/- 2%
NITROGEN	Balance		

Notes:

Approved for Release

Page 1 of 42-400196728-1

Figure A5 Airgas Certification of 250 ppm CO

Appendix – II

Evaluation Board Averaging Effects

As noted in Section 3.4, one feature of the software algorithm built-in to the e2v ECVQ-EK3 evaluation board is that it averages the sensor data for a minimum of one second before outputting an analog signal [23]. The impact of the e2v evaluation board only updating once a second is shown in Figure A6 which shows the output of the e2v EC4-500-CO sensor through the ECVQ-EK3 evaluation board as well as the Figaro TGS5042 sensor output through its COM5042 board. The response of both sensors is shown just after bladder rupture and exposure to the CO gas. Both sensors respond quickly. The Figaro TGS5042 exhibits typical signal-to-noise and no evidence of any on-board averaging routine. However, the e2v EC4-500-CO exhibits a clear stair-step pattern with a step-width of 1 second due to the on-board averaging algorithm.

The Figaro TGS5042 was also connected in series with a Keithley 195A Digital Multimeter to monitor the current output of the sensor directly. The sensor was placed in a test chamber and 116 mg/m^3 CO was flowed into the test chamber. The current measured by the digital multimeter directly from the sensor and the current measured by the COM5042 are shown in Figure A7. The current from the board follows the current from the sensor very closely. The COM5042 data were recorded at 10 Hz while the TGS5042 data were recorded at 0.2 Hz. The appearance of lower noise in the

TGS5042 data compared with the COM5042 data is a result of the lower data acquisition rate and not an inherit trait of the TGS5042 sensor compared with the COM5042 module.

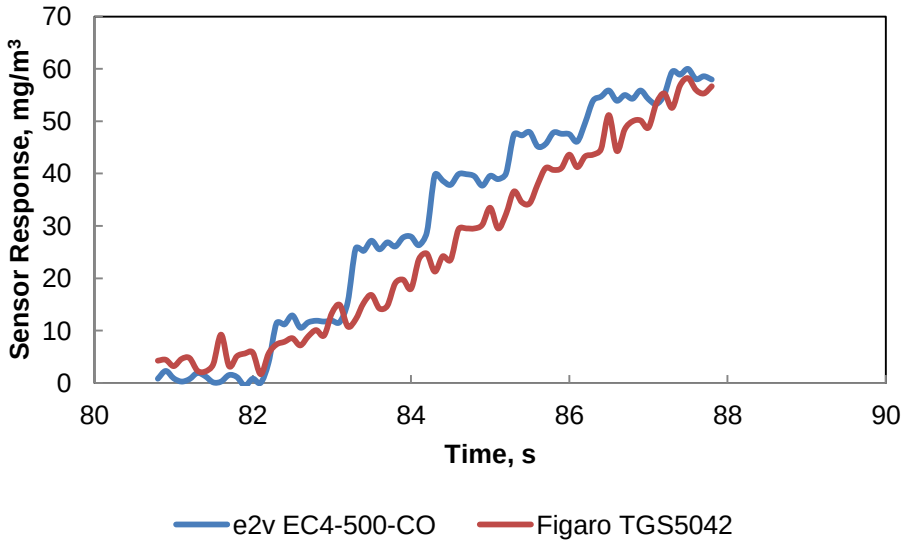

Figure A6: Response comparison between the e2v EC4-500-CO (blue) and Figaro TGS5042 (red). The e2v EC4-500-CO shows a step response while the Figaro TGS5042 is continuous.

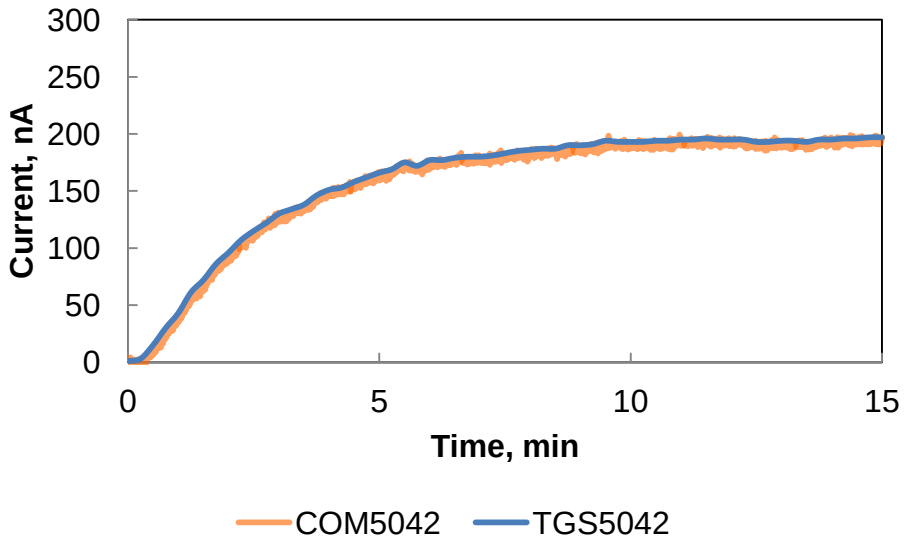

Figure A7: Current comparison between COM5042 and TGS5042. COM5042 was sampled at 10 Hz and TGS5042 was sampled at 0.2 Hz.

Appendix – III

Uncertainty Estimates

There are several sources of potential uncertainty in the measurements. These sources include possible temperature compensation, sensor drift, gas flow rate measurements, sensor linearity, zero current, repeatability, rounding, analyte concentration, and sensor interference with other gases [19]. Many of these uncertainty sources were minimized through experiment design and testing of the sensors. Temperature compensation was not an issue because all of the experiments, except the one elevated temperature set, were performed at room temperature (70 ± 2^{o}F). Potential problems with sensor drift were avoided by choosing very stable sensors and completing comparable tests within a few weeks to avoid any long term drift of the sensors. Gas flow rate issues were not important because the sensors were placed in still gas and the analyte allowed to diffuse into the sensor rather than the analyte being pumped into the sensor housing. The linearity, zero current and repeatability were minimized by the manufacturer and verified by the current set of experiments. Potential gas interference problems were minimized by applying a gas mixture that only contained CO and N_2. Sensor round-off effects and repeatable analyte concentrations were considered to be the main sources of uncertainty for these experiments.

The experimental design was chosen to isolate the sensor response for the transient analysis. The process of filling the bladder with CO leads to uncertainty in the calculation of CO concentration in the chamber. Twenty bladders were filled for 12 seconds to check the precision of the bladder fill volume. The results of the fill tests are shown in Table A1.

Table A1: Bladder volume results

Bladder	*Actual Fill Time*	*Volume (L)*
1	12.2	1.58
2	12.2	1.58
3	11.95	1.54
4	12	1.54
5	12.2	1.58
6	12.15	1.57
7	12.1	1.55
8	12.1	1.55
9	12.2	1.57
10	11.9	1.53
11	12.25	1.58
12	12	1.54
13	12.15	1.56
14	11.95	1.54
15	12.1	1.56
16	12.05	1.55
17	12	1.55
18	12.2	1.57
19	12	1.55
20	12.15	1.56
Average	*12.09*	*1.56*
Standard Deviation	*0.10*	*0.01*

The standard deviation of the fill time was 0.1 seconds and the standard deviation of the volume was 0.01 L. For a 95% confidence interval, the error in chamber concentration for bladders filled is shown in Table A2.

Table A2: Concentration uncertainty due to bladder fill

Concentration (mg/m^3)	*Error (mg/m^3)*
1	0.002
5	0.009
10	0.018
30	0.053
60	0.105
90	0.158
145	0.255

With consistent bladder fill times there is low error due to the differences in bladder fill.

Another source of error is the uncertainty in the measurement of the volume of the test chamber. The irregular shape of the test plug as well as the components placed inside the chamber contributes to this uncertainty. Figure A8 shows the desired chamber concentration and the range of actual concentrations assuming the uncertainty in the volume of the chamber is ±5% of the total volume. The range of concentrations increases as the concentration in the chamber increases indicating there is more uncertainty in the higher CO concentrations.

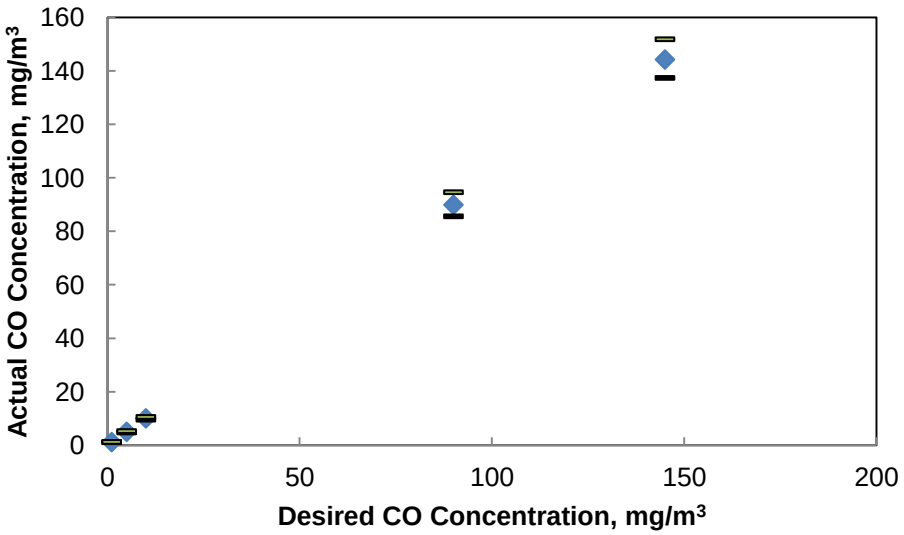

Figure A8: The actual CO concentration range as a function of the desired CO concentration. The diamond symbols indicate a known chamber volume and the bars indicate a ±5% volume uncertainty.

Appendix – IV

Sensor Rate of Response

The rate of response of the Figaro TGS5042 sensor was examined more closely. In Figure A9, the rate of response was plotted as a function of when the calculation of the rate began. The duration of rate calculation was varied from 3 to 10 seconds. The initial calculation start time was chosen as the moment that the detection limit was achieved (i.e., the moment the sensor signal reached 3 times the sensor RMS noise). The goal was to find a start time and length for the calculation that best represented the rate of response of the sensor. These calculations were performed for the experimental data of the Figaro TGS5042 exposed to a concentration of 60 mg/m^3 CO.

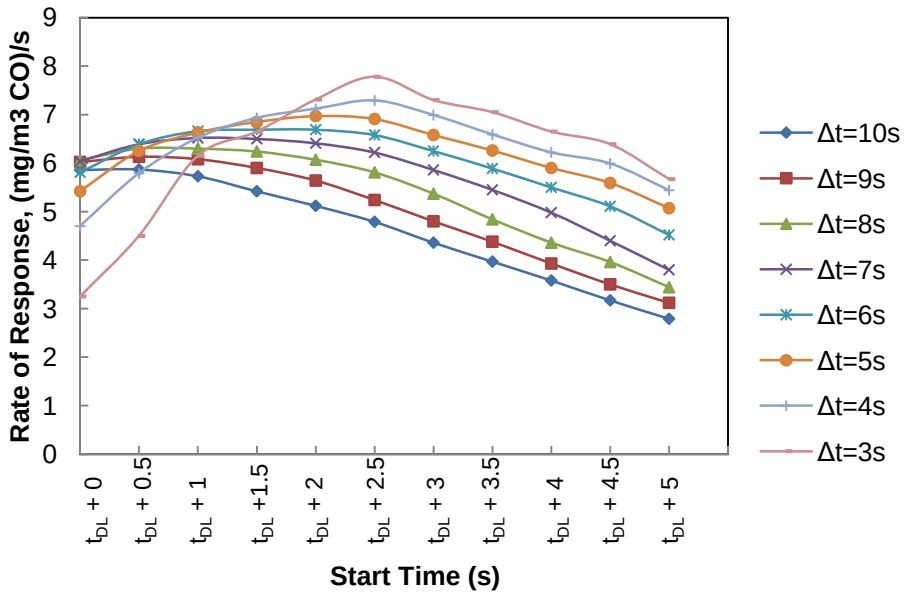

Figure A9: The rate of response is shown for the Figaro TGS5042 exposed to 60 mg/m^3 CO. The rate of response was calculated as a linear curve fit from a starting time of t_{DL} + x seconds for a Δt from 3 to 10 seconds.

The Figaro TGS5042 response to concentrations of 10, 30, 60, 90 and 145 mg/m^3 CO are shown in Figure A10-A14. The response for each and the first derivative of the response are shown. The sensor response data were filtered using a running average to compute the first derivative.

a

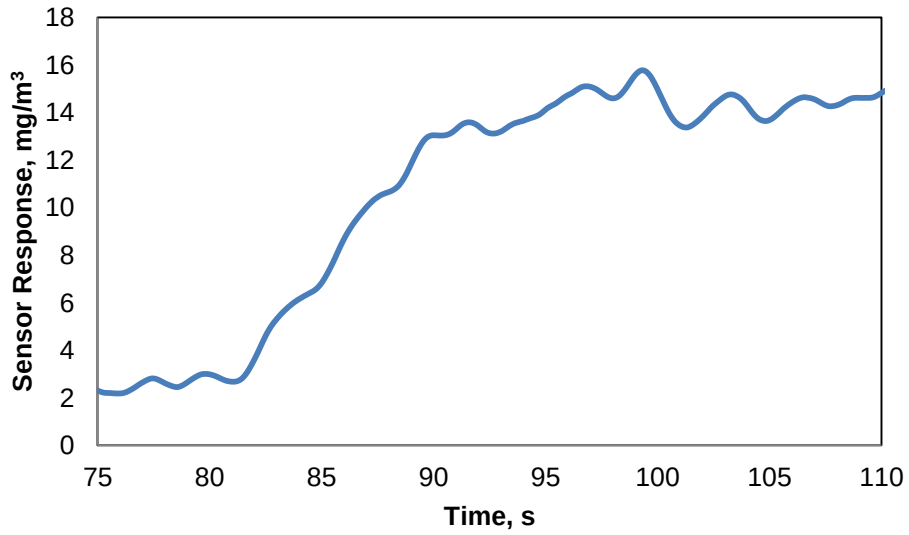

b

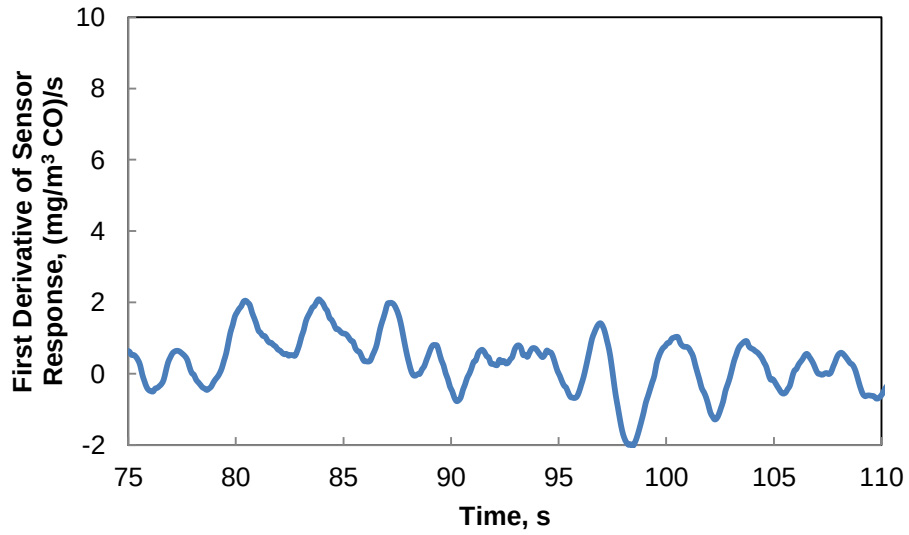

Figure A10: a) Figaro TGS5042 response to 10mg/m^3 CO b) First derivative of sensor response

a

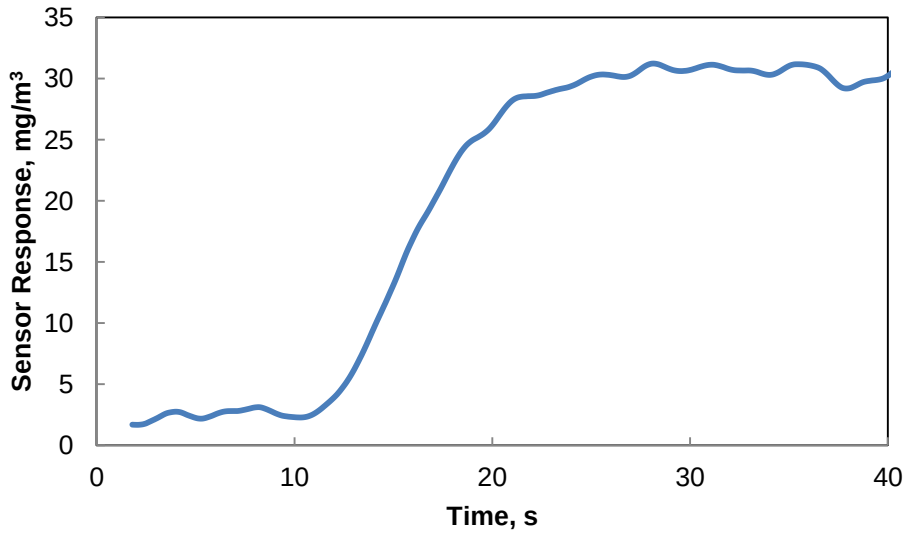

b

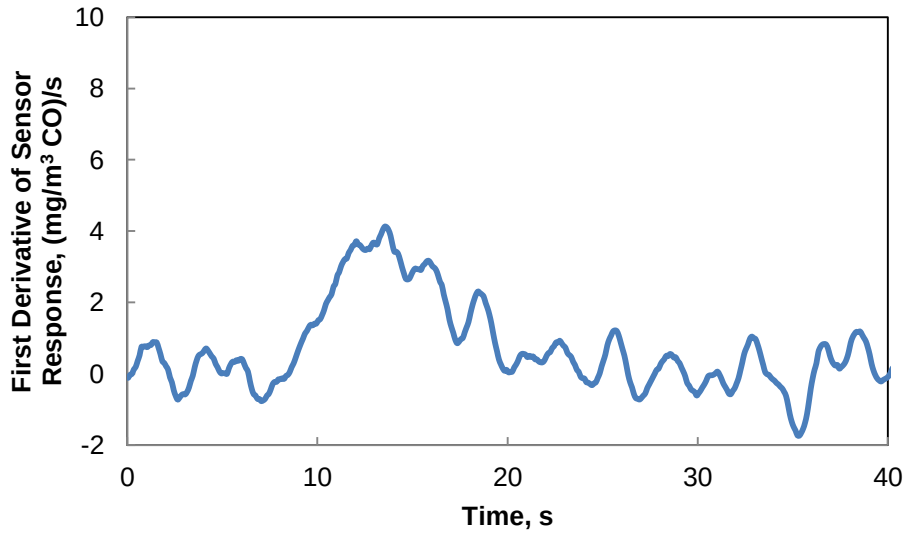

Figure A11: a) Figaro TGS5042 response to 30mg/m^3 CO b) First derivative of sensor response

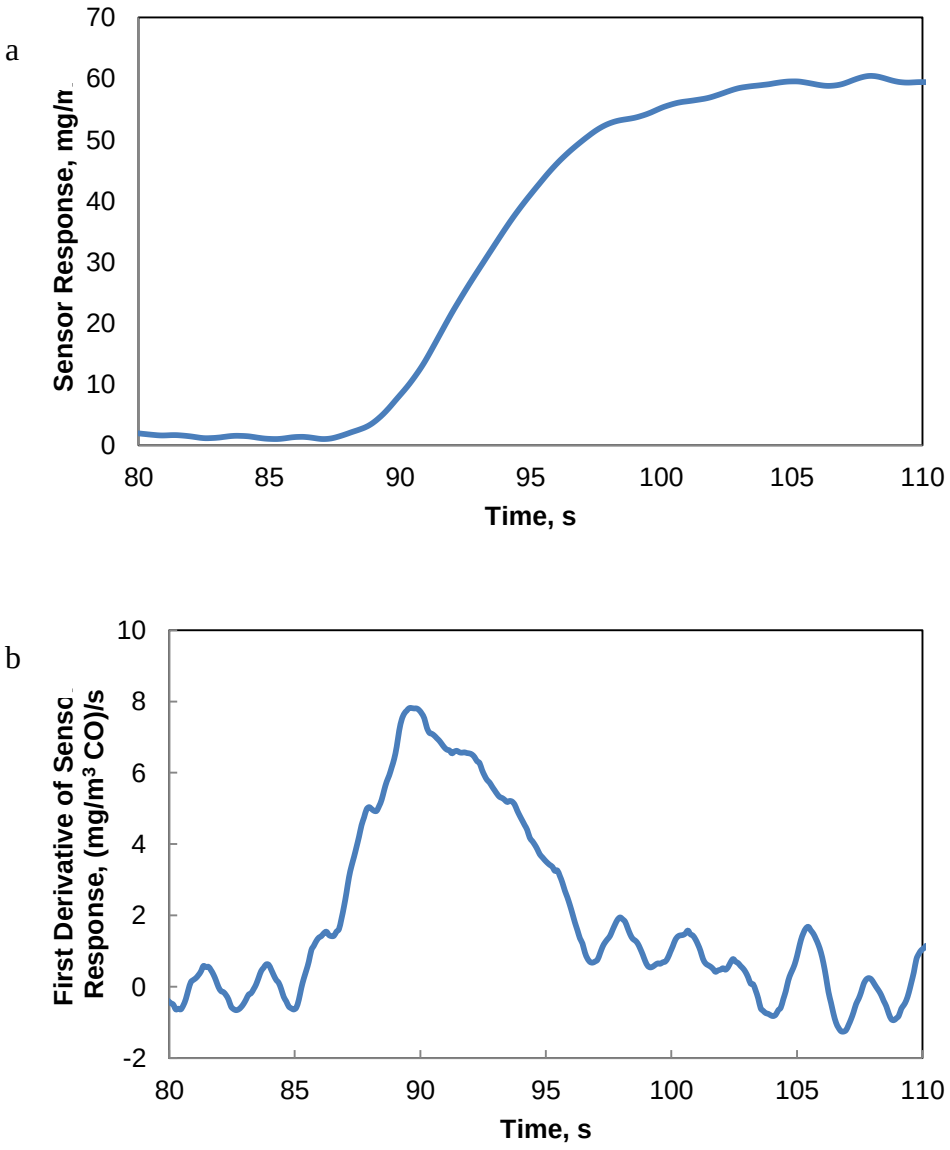

Figure A12: a) Figaro TGS5042 response to 60mg/m^3 CO b) First derivative of sensor response

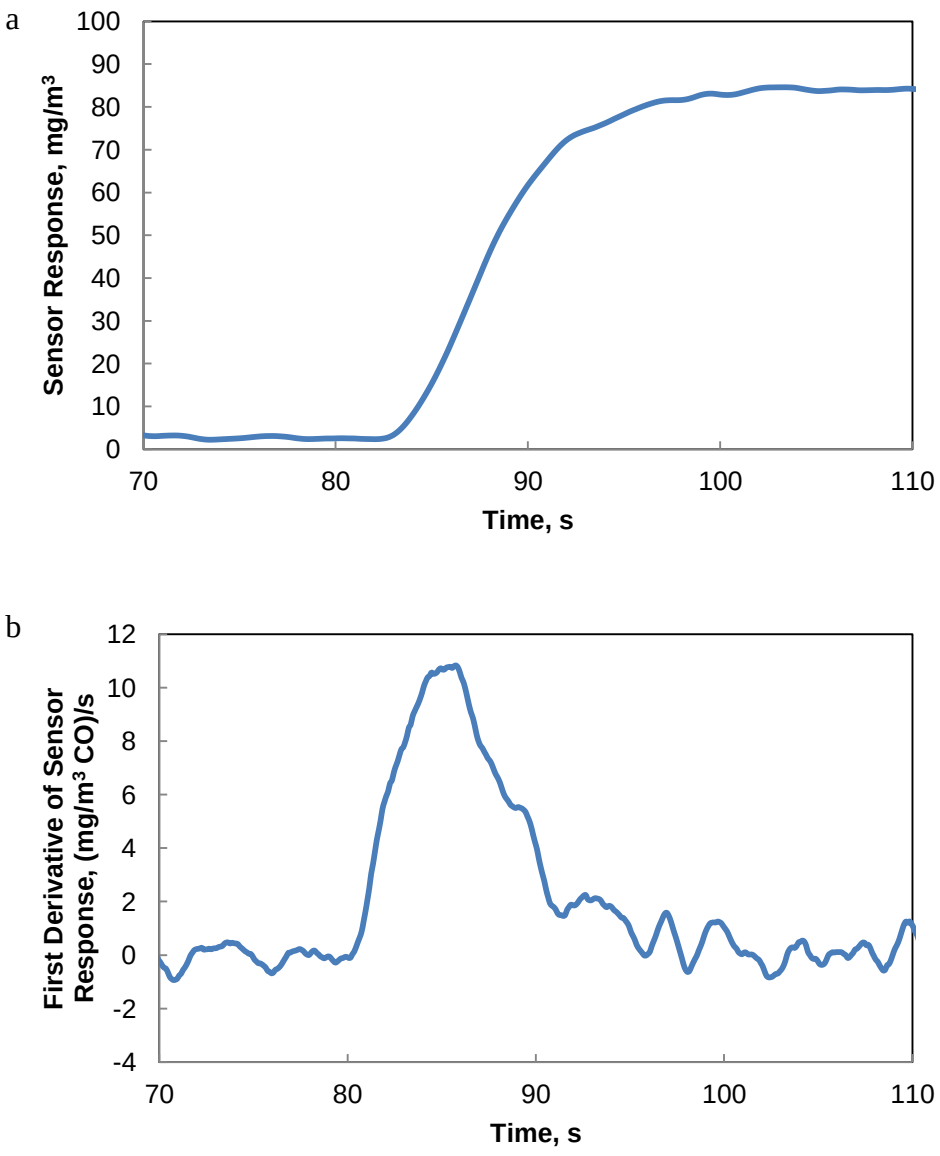

Figure A13: a) Figaro TGS5042 response to 90mg/m^3 CO b) First derivative of sensor response

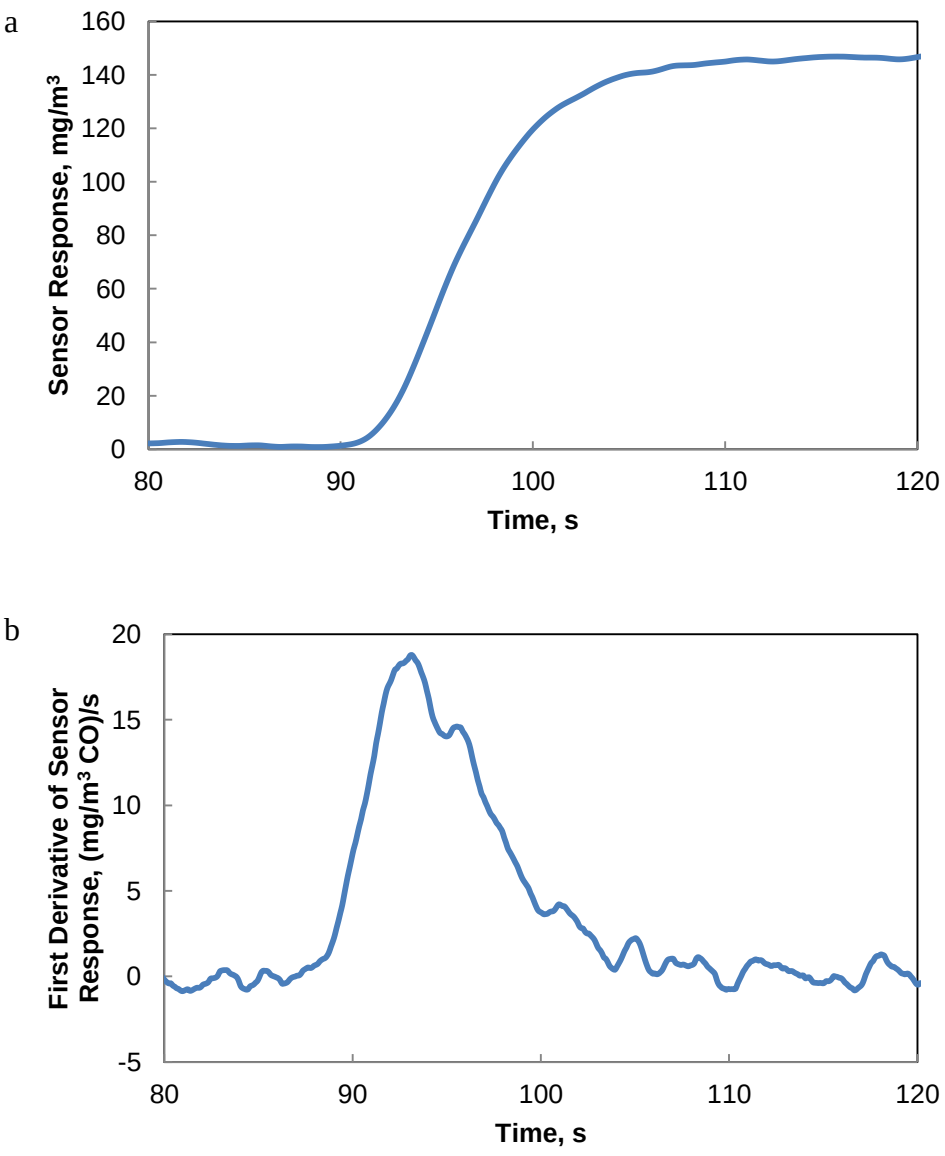

Figure A14: a) Figaro TGS5042 response to 145mg/m^3 CO b) First derivative of sensor response